Title
Crack Path and Fracture Energies in Ceramic-Metal Sandwich Geometries

Authors
Cannon, R.M.
Dalgleish, B.J.
Dauskardt, R.H.
et al.

Publication Date
1992-08-01

LBL-32868
UC-404
Preprint

Center for Advanced Materials

CAM

Submitted to Journal of the American Ceramic Society

Crack Path and Fracture Energies in Ceramic-Metal Sandwich Geometries

R.M. Cannon, B.J. Dalgleish, R.H. Dauskardt,
J.M. McNaney, and R.O. Ritchie

August 1992

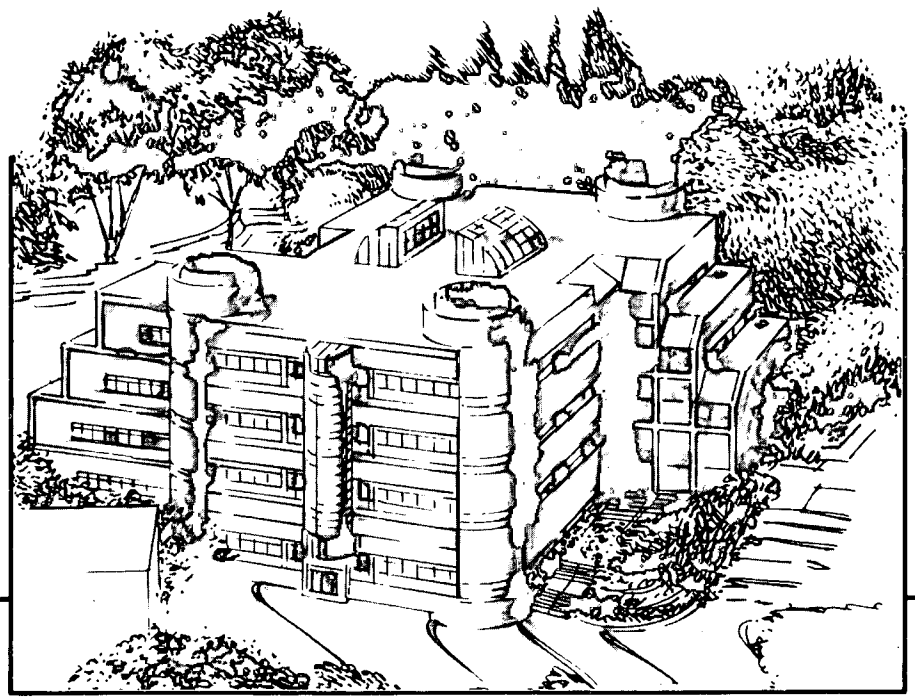

Materials and Chemical Sciences Division

Lawrence Berkeley Laboratory • University of California

ONE CYCLOTRON ROAD, BERKELEY, CA 94720 • (415) 486-4755

Prepared for the U.S. Department of Energy under Contract DE-AC03-76SF00098

DISCLAIMER

LBL-32868
UC-404

CRACK PATH AND FRACTURE ENERGIES IN CERAMIC-METAL SANDWICH GEOMETRIES

R. M. Cannon, B. J. Dalgleish, R. H. Dauskardt
J. M. McNaney and R. O. Ritchie

Center for Advanced Materials, Materials Sciences Division
Lawrence Berkeley Laboratory
and
Department of Materials Science and Mineral Engineering
University of California, Berkeley, CA 94720

August 1992

submitted to
Journal of the American Ceramic Society

This work was supported by the Director, Office of Energy Research, Office of Basic Energy Sciences, Materials Sciences Division of the U.S. Department of Energy under Contract No. DE-AC03-76SF00098.

CRACK PATH AND FRACTURE ENERGIES IN CERAMIC-METAL SANDWICH GEOMETRIES

R. M. Cannon, B. J. Dalgleish, R. H. Dauskardt
J. M. McNaney and R. O. Ritchie

Center for Advanced Materials, Lawrence Berkeley Laboratory, and
Department of Materials Science and Mineral Engineering
University of California, Berkeley, CA 94720

ABSTRACT

This paper examines the factors dictating the choice of crack path for ceramic/metal joints under monotonic and cyclic stresses, an issue which often controls the strength and toughness of such joints and hence the lifetime of many coatings, electronic devices and structural composite materials. Experimental results from fracture-mechanics tests on ceramic/metal/ceramic sandwich geometries are described which determine both the selection of crack path (i.e., in the metal, in the ceramic, or along the interface) and the corresponding crack-extension rates. It is found that the crack path is controlled both by the path of low microstructural resistance and the driving-force directionality, which itself is a function of the far-field loading and the elastic compliance mismatch across the interface. Critical factors include the interface chemistry, the loading type (cyclic vs. monotonic), the elastic properties of the metal and ceramic, and the role of constrained plasticity. Crack-tip fields based on the mismatch of elastic properties provide reasonable predictions of trends in many systems (glass/Cu, SiO_2/Cu, Al_2O_3/Al, Al_2O_3/Al-4Mg, Al_2O_3/Au, Al_2O_3/Cu, Al_2O_3/Pt), although corrections for plasticity are often required. Where the compliance mismatch takes the crack off the weak microstructural path, cracking configurations are invariably erratic and high toughness joints result. Similarly, high toughnesses are achieved where cracking occurs at, or near, both interfaces; such crack jumping is promoted by ceramic/metal bonds with varying interfacial strength or where crack-tip plastic zone sizes are comparable with the metal layer thickness.

I. Introduction

The mechanical behavior of ceramic/metal interfaces is often a key aspect of the performance of modern structural composite materials.[1] Equally important, the yield and

reliability of microelectronic and optical devices, sensors, actuators and their packages, and of coatings rely upon such interfaces.[2] Device lifetimes can be dictated by delayed fracture driven by residual stresses, thermal cycling and mechanical vibrations.[3-6] Time dependencies can reflect subcritical cracking enhanced by temperature (creep), moisture or corrosive species (stress corrosion), diffusion of same through encapsulation, stress relaxation, or cyclic loading induced crack extension (fatigue) *per se*. Extensive practical experience has led to refinements to reduce interfacial flaws, adverse reaction products and stress concentrations.[2,6,7] However, information about strength, fracture toughness and specifically crack growth along ceramic/metal interfaces and their metallurgical determinants has been inadequate for designing composites or devices. That situation is changing rapidly;[8,9] nevertheless, little effort has been devoted to such critical factors as the prediction of the crack path, which plays such a vital role in determining the integrity and hence the lifetime of a specific ceramic/metal bond.

Assessing failure and lifetimes generally entails treating the initiation and ensuing extension of one or more cracks to criticality or until devices malfunction. With brittle and ductile materials combined at ceramic/metal interfaces, crack initiation may involve both localized plasticity and prior flaws. Analyses for monotonic loading addressing stress concentrations and residual stresses near interfaces, and the constrained plasticity within metallic layers adjoining non-deforming materials[10-13] reiterate the sensitivity to geometry and the fabrication defect population. The interfacial fracture resistance is deemed to be a more fundamental characteristic, although it too depends on local microstructure and chemistry. However, the interface *per se* may not fail.

For example, glass/Cu samples invariably fail at the interface under monotonic loading with a low G_c of ~2-10 J/m^2, whereas fast interfacial fracture energies higher by one to three orders of magnitude, but still for interfacial failure, have been reported for bonds between alumina and Au, Pt, Cu and Nb.[14] These do not correlate directly with typical estimates of the interfacial chemical bonding or work of adhesion,[15] but the trends are toward finding higher toughnesses resulting from thicker metal layers and possibly lower yield stresses and rougher interfaces. Such

dependencies, however, have not been verified independently. Finally, alumina/Al samples, which exhibit relatively high G_c values, rarely failed exactly at the interface.[16] Thus, critical unresolved issues involve knowing where a crack will initiate, where it will go, and how long it will take to get there.

This paper addresses the second of these issues, specifically the factors dictating the choice of crack path for ceramic/metal joints subjected to either monotonic or cyclic stresses. Based on recently published linear-elastic interfacial and near-interfacial crack-tip fields and experimental behavior observed on ceramic/metal sandwich geometries, it is shown that reasonable predictions of the crack path can be made which provide preliminary guidelines for the design of ceramic/metal bonds with improved fracture energies.

II. Interfacial Fracture Mechanics

Interfacial fracture energies, or fracture toughnesses, G_c, measured for sundry oxide/metal systems[12-14,16-25] vary widely and are so sensitive to interfacial purity, orientation, morphology and adjoining microstructure that it is tenuous to attribute many aspects as inherent to the material pair comprising the interface. This interpretation, however, is clouded by variability in the geometry and crack-tip stresses which in part govern the crack path. Accordingly, we first focus on the stress and deformation fields developed at crack tips located at or near bimaterial interfaces, and the linear-elastic mechanics analyses governing the crack path and crack deflection.

(1) Crack-Tip Fields

An elastic compliance discontinuity at an interface modifies the stress fields for cracks at or near interfaces, as has been expressed using both linear elastic[26-29] and nonlinear elastic[30] fracture mechanics. Differences in elastic properties can cause the ratio of normal to shear stresses ahead of the crack to differ markedly from that expected from far-field loading. Characterizing this issue is important as the local stresses may dictate the preferred crack extension direction. If the interfacial bonding is "weak", the crack may follow the interface even under mixed

mode loading. With stronger interfaces, cracks will tend to deflect along a $K_{II} = 0$ trajectory, as occurs in homogeneous (brittle) materials;[29] the fracture resistance will then depend upon the crack path and the amount of shear at the crack tip.

Cracks at interfaces: For a crack on an interface separating two isotropic, homogeneous, elastic solids, the near-tip stress-intensity factor K is most conveniently expressed in complex notation using the near-tip stress intensities such that $K = K_1 + iK_2$ (where $i = \sqrt{-1}$). K describes important aspects of the local field and is related to the strain energy release, *G*, as:

$$G = \left(1-\beta^2\right)\left(K_1^2 + K_2^2\right)\frac{1/E_1^{'} + 1/E_2^{'}}{2} \quad , \tag{1}$$

where $E_i^{'}$ are Young's moduli in plane stress or $E_i/(1-\nu_i^2)$ in plane strain, ν_i are Poisson's ratios, and the subscripts 1 and 2 for material properties refer to the solids above and below the crack, respectively (Fig. 1a). The moduli mismatch effects on crack-tip fields can be described using two non-dimensional (Dundurs' elastic mismatch) parameters,[31] α and β; in plane strain:

$$\alpha = \frac{E_1^{'} - E_2^{'}}{E_1^{'} + E_2^{'}} \quad , \tag{2a}$$

$$\beta = \tfrac{1}{2}\left\{\frac{\mu_1\left(1-2\nu_2\right) - \mu_2\left(1-2\nu_1\right)}{\mu_1\left(1-\nu_2\right) + \mu_2\left(1-\nu_1\right)}\right\} \quad , \tag{2b}$$

where μ_i are the shear moduli; both α and β vanish when the elastic mismatch does. Dundurs' parameters for a wide range of dissimilar material combinations in plane strain are plotted in α-β space[32] in Fig. 2; examples are primarily taken for metals bonded to alumina, silicon and silica glass. A listing of the values of α and β for the ceramic/metal systems studied in the present work is given in Table I.

Table I: Modulus Mismatch Parameters for Ceramic/Metal Couples Studied

Material Pair #1/#2	Dundurs' Parameters α	β
Glass/Cu	-0.329	-0.154
Alumina/Al	+0.686	+0.143
Alumina/Au	+0.644	+0.049
Alumina/Cu	+0.490	+0.087
Alumina/Pt	+0.423	+0.027

Using these definitions of α and β, the interface stress intensity can then be expressed as:

$$K_1 + i\,K_2 = g(\alpha,\beta)\left(K_I^{\infty} + i\,K_{II}^{\infty}\right)L^{-i\varepsilon}\,e^{i\omega(\alpha,\beta)}\ , \tag{3}$$

where g(α,β) is a geometry specific function of the elastic mismatch. The "phase shift" function ω, which depends upon α, β and geometry, describes the stress field rotation at a specified distance L from the crack tip, relative to that expected from mode I and mode II stress intensities, K_I^{∞} and K_{II}^{∞}, that describe the far-field, in-plane loading. Recent solutions for ω use $L = h_2$, the thickness of the metal film for thin film or ceramic/metal/ceramic sandwich geometries.[33,34] The loading mode can be characterized in terms of the ratio of shear to normal tensile stresses acting on the interface at some distance x from the crack tip, and expressed as a phase angle,[29] i.e.,

$$\psi(x) = \tan^{-1}\left(\frac{\sigma_{xy}}{\sigma_{yy}}\right)_x = \tan^{-1}\left(\frac{Im\left(Kx^{i\varepsilon}\right)}{Re\left(Kx^{i\varepsilon}\right)}\right)\ , \tag{4a}$$

$$\psi(x) = \tan^{-1}\left(\frac{K_{II}^{\infty}}{K_I^{\infty}}\right) + \omega(\alpha,\beta;L) + \varepsilon ln\left(\frac{x}{L}\right)\ . \tag{4b}$$

The near-tip variability depends only upon β via the oscillation index:

$$\varepsilon = \frac{1}{2\pi} \ln\left(\frac{1-\beta}{1+\beta}\right) . \qquad (5)$$

As defined in refs. 26-29, K_1 and K_2 are indeterminate if $\beta \neq 0$, but interfacial crack-tip stresses and Eq. (1) are unique in terms of far-field loads and dimensions. Using the notion of Fig. 1a for an elastic bimaterial interface, these stresses are given in terms of radial distance r from the crack tip by:[26,27]

$$\sigma_{ij} = \frac{1}{\sqrt{2\pi r}}\left[Re\left(Kr^{i\varepsilon}\right)\tilde{\sigma}_{ij}^{I}(\theta,\varepsilon) + Im\left(Kr^{i\varepsilon}\right)\tilde{\sigma}_{ij}^{II}(\theta,\varepsilon)\right] + T\delta_{ij}\delta_{ji} + O\left(\sqrt{r}\right) , \qquad (6)$$

where i,j = x,y, and the dimensionless angular functions $\tilde{\sigma}_{ij}^{I}(\theta,\varepsilon)$ and $\tilde{\sigma}_{ij}^{II}(\theta,\varepsilon)$ are related to the tractions across the interface and are given in ref. 27. The specimen geometry dependent T term is a non-singular stress acting parallel to the crack plane and is approximately constant for large distances behind and in front of the crack tip.[35] The T-stress of the σ_{xx}-component has an important bearing on crack stability and kinking.[36] For cracks at bimaterial interfaces, the σ_{xx}-component of the thermally-induced residual stresses may be expected to produce a similar effect. In fact, the residual stress contribution to the T-stress has recently been identified to be one half of the nominal residual stress, σ_{xx}^{res}:[37]

$$T = \tfrac{1}{2}\sigma_{xx}^{res} = \tfrac{1}{2}E^{*}\Delta\alpha\Delta T , \qquad (7)$$

where E^* is the mean Young's modulus of the two materials, $\Delta\alpha$ is the difference in thermal expansion coefficients, and ΔT is the temperature change. According to Schmauder and Meyer,[38] consideration of such residual stresses can significantly increase the mode mixity and effective stress intensity at the tip of interface cracks.

Cracks near interfaces: For a sandwich geometry consisting of two linear-elastic materials subjected to remote loads K_I^{∞} and K_{II}^{∞}, where a layer of material 2 (thickness h_2) is sandwiched

between identical blocks of material 1 (Fig. 1b), if the inner metal layer thickness is small compared to other in-plane crack dimensions, the strain energy release rate for a crack within the layer is given by:[33,39]

$$G = \left(\frac{1}{E_2'}\right)\left[K_I^2 + K_{II}^2\right] = \left(\frac{1}{E_1'}\right)\left[\left(K_1^{\infty}\right)^2 + \left(K_{II}^{\infty}\right)^2\right] , \tag{8}$$

where the local stress intensities, K_I and K_{II}, can be expressed as:

$$K_I + i K_{II} = \left[\frac{1-\alpha}{1+\alpha}\right]^{1/2}\left(K_I^{\infty} + i K_{II}^{\infty}\right)e^{-i\phi} . \tag{9}$$

Here ϕ can be interpreted as the phase angle shift between the remote and local stress intensities, viz.:[39]

$$\phi = \tan^{-1}\left(\frac{K_{II}}{K_I}\right) - \tan^{-1}\left(\frac{K_{II}^{\infty}}{K_I^{\infty}}\right) . \tag{10}$$

For cracks close to the interface, i.e., where h_2/a and $c/h_2 \ll 1$ in Fig. 1b, Eq. (10) becomes:[28]

$$K_I + i K_{II} = \left[\frac{1-\alpha}{1+\alpha}\right]^{1/2}\left(K_I^{\infty} + i K_{II}^{\infty}\right)\left(\frac{c}{h_2}\right)^{-i\varepsilon} e^{-i(\phi h+\omega)} , \tag{11}$$

where an approximate yet highly accurate solution for ϕ is given by:

$$\phi = \varepsilon ln\left(\frac{h_2 - c}{c}\right) + 2\left[\left(\frac{c}{h_2}\right) - 1/2\right]\left[\phi_h(\alpha,\beta) + \omega(\alpha,\beta)\right] , \tag{12}$$

and the functions $\phi_h(\alpha,\beta)$ and $\omega(\alpha,\beta)$ are tabulated in Refs. 28 and 33, respectively.

For cracks within the layer, as with traction-free isotropic solids subjected to remote mode I and mode II stress intensities, the T-stress which acts parallel to the crack plane affects the stability and kinking yet does not induce a stress intensity at the crack tip; this follows because T

(and the σ_{xx}-component of the residual stress in the layer) cause no tractions on any plane parallel to the layer.[39]

It should be noted, however, that many results from such sandwich samples involve a very thin layer of metal between two much larger ceramic blocks (Fig. 3). In this case, residual stress effects are minimized and the computation of G from test results is direct as the strain energy in the ceramic is little perturbed by the thin layer; G can thus be simply computed from the far-field loading as:

$$G = \frac{\left(K_I^{\infty}\right)^2 + \left(K_{II}^{\infty}\right)^2}{E_1^{'}} \quad , \tag{13}$$

where $E_1^{'}$ is the Young's modulus of the ceramic layer.

III. Crack-Path Selection

The trajectory of a crack in a homogeneous, or dissimilar material layered, structure is controlled by the mutual competition of two primary factors: the direction in which the fracture-mechanics driving force is highest and the direction where the microstructural resistance is lowest. Each of these considerations is discussed below with reference to fracture *at* or *near* ceramic/metal interfaces in sandwich structures.

(1) Mechanics Considerations

Crack-path preference has been analyzed in terms of stability to kinking as dictated by the local loading mode, ψ.[29] In layered or sandwiched structures as with homogeneous solids, under linear elastic conditions, cracks will tend to deflect along a path, or kink angle, defined by the maximum strain energy release rate G_{max}. However, recent analyses[29] have shown that for all practical purposes, this crack-path selection criterion based on maximizing G is identical to one

based on propagation in the direction where the Mode II stress intensity is zero, i.e., along a $K_{II} = 0$ path.*

*The angle through which a crack deflects to maximize G is essentially identical to that for which $K_{II} = 0$, except where the far-field loading is strongly mode II or where the crack kinks into a much stiffer material. The distinction between the two criteria, however, is very small; only above phase angles of $\psi \sim 50°$ is the difference more than one degree.[29]

Cracks at interfaces: Crack trajectories resulting from the modulus mismatch, which is defined by the values of α and β for a given bimaterial combination,[28,40] are anticipated from these analyses. For example, since the driving force for a crack on an interface between two linear-elastic materials #1 and #2 (Fig. 1a) is to follow the G_{max} (or $K_{II} = 0$) path, under applied mode I loading ($K_{II}^{\infty} = 0$) loading, the crack-tip field solution (Eq. 3) implies that when $\beta = 0$ the crack will kink upwards into material #1 regardless of the sign of α. However, when $\alpha = 0$, the crack will kink upwards into material #1 when $\beta < 0$ and downwards into material 2 when $\beta > 0$.

In order to decide whether the interface crack will deflect along the highest driving force path ($K_{II} = 0$) and into material #i, the ratio of maximum driving force (G_{max}) to that for continuing along an interface (G_{IF}), must be considered.[40] These provide a basis for a provisional criterion for a crack to leave a strong enough interface; i.e., kinking will occur if:

$$\frac{G_{\max}}{G_{IF}} > \frac{G_{ci}}{G_{cIF}} \quad , \tag{14}$$

where $G_{ci}/G_{cIF}(\psi)$ gives the relative fracture resistances for extension along the two paths under the specific loading. However, for many multilayer applications, plasticity within the metal encompasses dimensions which are comparable to the layer thickness or to incipient kink sizes, which may invalidate, or at least complicate, the elastic analysis.

Cracks near interfaces: Considering first the nature and stability of the crack path in layered or sandwich structures where the crack exists near an interface,[39] such as that depicted in Fig. 1b, under pure mode I far-field loading ($K_{II}^{\infty} = 0$), linear-elastic analysis would dictate that a straight crack within the central layer #2 would sit along the centerline ($c/h_2 = 0.5$) to satisfy the $K_{II} = 0$

condition*. For a crack above the centerline, kinking down toward the centerline will occur if $K_{II} > 0$. In general terms, this implies that straight cracks misplaced from the centerline (i.e., the $K_{II} = 0$ path) will only head toward the centerline if the K_{II}-gradient is positive, i.e., $\partial K_{II}/\partial c > 0$. If $\partial K_{II}/\partial c < 0$, the negative K_{II} will drive the crack away from this preferred path and the crack will kink toward the interface. However, as shown below, with certain layered material combinations, an additional straight crack path satisfying the $K_{II} = 0$ criterion is found away from the centerline close to one of the interfaces.

*To preserve stability along this centerline path, an additional necessary condition is that a *compressive* T-stress exists.[39] In the presence of a positive T-stress, there is a tendency for this crack path to become unstable.[36]

For a given structure under applied (far-field) mode I or mixed-mode loading, the location of the preferred $K_{II} = 0$ crack paths, and the sign of the K_{II}-gradient $\partial K_{II}/\partial c$ there, can be determined from the relevant crack-tip field solutions for near-interface cracks[28] and sandwich layers,[33] e.g., Eq. (9). For the bimaterial layered structures under consideration (Fig. 1b), these factors depend solely upon the elastic mismatch parameters α and β. Thus, using this approach and assuming that linear-elastic conditions prevail, it is possible to predict the likely crack path for all bimaterial combinations in terms of their relative elastic moduli and Poisson's ratios.

For the pure mode I far-field loading employed in the present study, the location c/h_2 of the crack within the metal layer #2 for which $K_{II} = 0$, and the nature of the K_{II}-gradients both inside and outside the layer, were determined from Eq. (9) in terms of all possible combinations of α and β. Three types of cracking configurations satisfying $K_{II} = 0$ are found; these are illustrated graphically in Fig. 4.

For $\beta < 0$ with any value of α, as shown by the lighter hatched region in Fig. 3, the centerline of the metal layer satisfies $K_{II} = 0$ but is an unstable path in the sense that $\partial K_{II}/\partial c < 0$. Accordingly, the driving force for cracks pre-existing within the metal layer will tend to deflect these cracks toward the interface, whereas near-interface cracks in the ceramic substrates will have the tendency to deflect away from the interface. This behavior should be shown by

geometries consisting of metal layers sandwiched between more compliant glass substrates (e.g., a Cu layer sandwiched between glass or silicon substrates).

For $\beta > 0$, the centerline of the metal layer again satisfies $K_{II} = 0$, but the gradient $\partial K_{II}/\partial c$ in this vicinity is only positive for the range of values of α shown by the darker hatched area in Fig. 4. In this regime, the crack should seek the center of the metal layer; if it lies off center within the metal layer, it should kink toward the centerline because of the positive K_{II}, whereas if it pre-exists outside the layer in the substrate, it should be drawn into the interface. Examples of this behavior should be seen with metal layers sandwiched between stiffer ceramic substrates, such as Al_2O_3-Cu and Al_2O_3-Al.

For the remaining values of α with $\beta > 0$, shown by the two unhatched regions in Fig. 4, cracks outside the metal layer in the substrates should still be drawn by the positive K_{II}-gradient into the interface; however, for cracks existing within the metal the situation is different. Three locations within the layer satisfy $K_{II} = 0$: the centerline at $c/h_2 = 0.5$, but this represents an unstable path in the sense that $\partial K_{II}/\partial c < 0$, and two other locations close to the interface where $c/h_2 \rightarrow 0$ or 1, both of which are stable as $\partial K_{II}/\partial c > 0$. In this regime, which should be seen in Al_2O_3-Au and Al_2O_3-Pt, cracks should follow at trajectory in the metal parallel but close to the interface.

Finally, it should be noted that the preferred crack-path trajectories specified in Fig. 4 pertain to linear-elastic conditions. Moreover, as described above, such trajectories may become wavy and unstable in the presence of a tensile T-stress, although plasticity within the metal layer would tend to negate this effect.

(2) Microstructural Crack -Growth Resistance

An alternate view emerges from simple models[13,21,41] relating interface bond-rupture resistance, yield stress and crack path. Expected trends are depicted in Fig. 5 as the dependence of fracture energy, G_c, upon metal yield strength, σ_y, in the limits where the interface bonding is "weak" or "strong", i.e., such that at high yield stress, failure would be at the interface or in the

ceramic, respectively. If the yield stress is low, fracture will proceed via ductile rupture within the metal, whilst crack blunting diminishes the crack-tip stresses to a small multiple of the metal flow stress and, thereby, precludes attaining local stresses sufficient to drive cracking elsewhere. Then, if the metal layer is thinner than the natural crack-tip plastic zone, the fracture energy will be smaller the thinner the metal. In the interfacial fracture regime, plastic deformation contributes a majority of the fracture energy for most oxide/metal interfaces; the extent of plasticity depends inversely on the yield stress and is leveraged by the bond scission resistance at the crack tip, which, in turn, is influenced by interfacial and environmental chemistry.

Although details have not been rigorously affirmed by analysis or experiment, examples exist of behavior for each of the regimes. Bonds of glass/Cu, SiO_2/Cu, Al_2O_3/Au, Al_2O_3/Pt, or Al_2O_3/Nb usually fail at the interface over a wide range of energies.[14,21-25,42] Alternatively, a series of Al_2O_3/Al-metal flexure samples virtually never cracked at the interface (Fig. 6); with pure Al, failure was within the metal, whereas with Al-4%Mg alloy, fracture was primarily within the ceramic.[12,42] Below we outline elements for refined criteria for crack-path selection that incorporate concepts of the microstructural resistance to fracture and as well as the mechanical crack driving force, and further show where the elastic analyses need to be modified to incorporate nonlinear as well as linear deformation effects.

IV. Experimental Procedures

(1) Sample Preparation

Several ceramic/metal interface systems were studied, namely SiO_2 and soda-lime glass bonded to Cu and Al_2O_3 bonded to Al, Al-4wt%Mg alloy, Au, Cu and Pt. Mechanical characterization of these interfaces employed several sandwich-type fracture mechanics specimens, namely, double-cantilever beams (DCB), unnotched and notched 3- and 4-point bend (flexure) beams, and compact-tension C(T) specimens* (Fig. 3).

*Note that these specimen geometries develop quite different T-stresses, which as stated above does influence crack stability. Numerical calculations[35] for bend and compact samples of homogeneous material estimate values of T, normalized with respect to $K_I^\infty/\sqrt{a}$, to be 0.033 and 0.291, respectively. However, since in the current sandwich geometries, processing procedures dictate that a state of residual tension will invariably exist within the metal layer, values of the T-stress in the present experiments will be positive in all geometries.

Glass/Cu and SiO_2/Cu: Initial crack-growth studies on glass/Cu interfaces were performed on double-cantilever-beam (DCB) specimens, comprising thin, 99.99% purity, copper films evaporated onto two Corning high alkali glass, or pure silica, plates (of size 5x25x2 mm) and pressure diffusion bonding the two films together for 2.5 hr at 9 MPa and 450°C.[14,17,19] Masking provided an interfacial pre-crack; loading grips were attached by epoxy (Fig. 3a). The total metal layer thickness was ~1.5 μm such that the ratio of thicknesses of ceramic to metal, h_1/h_2, exceeded ~1000. Subsequent crack-path studies were performed with unnotched bend beams consisting of a ~125 μm layer of copper, solid-state bonded (for 48 hr at 1 MPa and 535°C *in vacuo*) between two glass beams (of size 8x4x30 mm); these samples had a h_1/h_2 thickness ratio of ~200 (Fig. 3c).

Al_2O_3/Al and Al_2O_3/Al-Mg: Studies on alumina/pure aluminum and alumina/Al-4Mg alloy interfaces utilized both compact-tension C(T) (Fig. 3b) and notched and unnotched bend specimens. The bonds were formed by the direct liquid-state, or solid-state, bonding of layers of 99.999% purity Al, or an Al-4wt%Mg alloy, between two substrates of Coors 99.5% purity Al_2O_3. Sheets of the Al material, ranging in thicknesses from 25 to 500 μm and emplaced between two diamond ground and polished alumina pieces, were heated above the melting point of the metal (5 min at 980°C) in a purified argon atmosphere to achieve liquid-state bonding.[16] Alternatively, the sandwich component was bonded in the solid state at 645°C *in vacuo* under a pressure of 2 MPa for 48 hr. C(T) specimens were machined from the bonded blocks to dimensions 25x24x3 mm, and subsequently polished. The thickness ratio h_1/h_2 was ~50. Bend samples (of size 3x3x25 mm) were prepared in similar fashion with the metal layer thickness varied between 25 and 500 μ m to give a thickness ratio exceeding ~25.

Al_2O_3/Cu, Al_2O_3/Au and Al_2O_3/Pt: Studies on alumina/copper, alumina/gold and alumina/platinum interfaces involved C(T) and unnotched 3- and 4-point bend specimens of similar

size to those used for Al_2O_3/Al. The ceramic-metal joints were formed by solid-state bonding of 25 to 250 μm thick sheets of 99.99% purity metal between substrates of Coors 99.5% purity Al_2O_3 *in vacuo* for between 12 and 24 hr; temperatures of 1040°C for Al_2O_3/Cu and Al_2O_3/Au and 1450°C for Al_2O_3/Pt were used. The thickness ratio h_1/h_2 of these samples varied from approximately 500 to 1000.

(2) Test Methods

DCB and C(T) samples were tested on computer-controlled high-resolution electro-servo hydraulic testing machines, operating in an environment of room air at 22°C with 45% relative humidity; crack-path morphologies were determined following stress-corrosion, cyclic fatigue-crack propagation or resistance-curve tests, with cracking initiated from a fatigue or pre-existing pre-crack. Full details of the respective testing procedures are given in Refs. 16,43,44. Bend samples were either unnotched or prepared with an array of Vicker's hardness indents (9½ kg load) across the highly polished tensile surface to simulate a notch. The beams were tested in a specially constructed ultrahigh stiffness rig with precision control on displacement to within 0.1 μm and on load to within 0.04 N; specimens were loaded under displacement control at a rate of 5 μm/min (notched) to 50 μm/min (unnotched) and the crack path determined. Where notches or pre-cracks were used, they were put in nominally at the center of the metal layer. In one series of bend tests on Al_2O_3/Al ($\beta > 0$) and glass/Cu ($\beta < 0$) interfaces, however, a series of Knoop hardness indents was made at varying distances from the interface in the ceramic. For Al_2O_3/Al samples, this simulated notch was placed at distances of $2h_2$, $3h_2$, $5h_2$ and $6h_2$ from the interface, where h_2 (~ 100 μm) is the thickness of the metal layer; in the glass/Cu specimens where h_2~125 μm, the notch was placed at distances of $1h_2$, $2h_2$ and $3h_2$ from the interface.

Where crack-growth rates were measured in DCB glass/Cu samples, crack monitoring was achieved optically or with a traveling microscope via interference fringes seen through the glass.[17] In C(T) specimens, ~0.1 μm thick NiCr films were evaporated onto the specimen face (with an insulating under-layer of ~0.4 μm thick sputtered alumina) and electrical measurements of the

resistance change across the NiCr film made to give an *in situ* resolution of crack lengths to within ±2 μm (Fig. 3b).[16,44]

Driving forces were evaluated in terms of both the far-field values of K and G. For all specimen geometries, the loading was symmetrical and the metal film thickness was much less than the crack length, a, or ceramic thickness, h_1; thus, the G values in terms of applied loads, P, are identical to those for homogeneous samples, under mode I far-field loading. For the DCB specimen geometry:[45]

$$G = \frac{12 P^2 a^2}{E_1' h_1^3 B B_n}\left[1+\frac{2h_1}{3a}\right]^2, \tag{15}$$

where the subscript 1 refers to the ceramic beam, h_1 is the beam half height, B, the beam thickness, and B_n, the crack-front thickness. For the C(T) sample, K_I is given by handbook solutions in terms of the crack-length to specimen-width ratio, a/W,[46] from which, using Eq. 13, G is:

$$G = \left[P^2 / E_1' B^2 W\right] f\left(a/W\right), \tag{16}$$

where

$$f\left(a/W\right) = \left\{\left[2+\left(a/W\right)\right]\left[0.886+4.64\left(a/W\right)-13.32\left(a/W\right)^2+14.72\left(a/W\right)^3-5.6\left(a/W\right)^4\right]\right\} / \left[1-\left(a/W\right)\right]^{3/2}$$

Resulting toughness G_c values for the various systems under study are listed in Table II.

Table II. Toughness Associated with the Fracture of Ceramic/Metal Couples

Material Pair #1/#2	Test Method	Fracture Location	Toughness, G_c (J/m^2)	Plastic Zone, r_y Size† (μm)
Glass/Cu	DCB	interfacial	2	0.31
SiO_2/Cu	DCB	interfacial	10	1.3
Al_2O_3/Cu	SEN(B)	interfacial	150	520
Al_2O_3/Al	4-pt BEND	metal	65-400	270-1600
Al_2O_3/Al-4Mg	C(T)	metal & ceramic	100-400	40-160

† estimated using Eq. 18

Although cracks in all geometries extend under virtually pure applied (far-field) mode I loading conditions, the elastic discontinuity across the interface induces a shear component. For example, for the glass/Cu bonds, the metal is rather stiffer ($\alpha < 0$), whereas for the alumina/metal C(T) samples, the metal is much less stiff ($\alpha > 0$); accordingly, the rotation angle[33] ψ, at a distance $x = h_2$ is +2° and -9°, respectively for interface cracks in these two bimaterial systems.

V. Experimentally Observed Crack-Path Morphologies

In general, a crack kinking off a ceramic/metal interface down into the metal (e.g., Fig. 6) usually has a higher driving force, G, when $\psi > 0$, and conversely if $\psi < 0$. However, for $\beta = 0$, a negative rotation angle leads to a maximum G for crack advance along the interface itself in the sandwich specimen. Moreover, analyses, based on that of He and Hutchinson,[40] reveal the $K_{II} = 0$ path to promote kinking away from the layer, regardless of the sign of α. The effects of $\beta \neq 0$ are clearer from combining the analyses for near-interface cracks[28] and sandwich layers[33]; as stated above, this yields that a crack in the ceramic would be attracted to the interface by $\beta > 0$ and would kink away for (Fig. 3). This would explain a tendency for cracks initiated in the stiffer alumina to be drawn toward the metal layer ($\beta > 0$), as described below. Once there, if the interface is "strong" and the metal tough, further advance may be erratic in path and load, e.g., plucking out bits of ceramic and deforming the metal giving high toughness.[42,47] Conversely, for SiO_2/Cu/SiO_2 samples, the fact that $\beta < 0$ should drive a crack into the glass if the interface is strong. We examine these scenarios by experiments below by considering cases of the "weak" interface, "weak" metal, and "weak" ceramic.

(1) "Weak" Interface

The presence of "weak" interface generally results in interfacial failure. In the present study, such behavior was invariably shown by glass/Cu bonds, where $\beta < 0$, and depending on the processing, on occasion by Al_2O_3/Cu, Al_2O_3/Au and Al_2O_3/Pt bonds, where $\beta > 0$. However, with

somewhat better bonding, particularly with a tougher metal, or following interactions with defects in the vicinity of the interface, the interfacial cracks in these systems often deflect into the ceramic, with their subsequent behavior depending upon the sign of β.

For the glass/Cu bonds in the current work, catastrophic fracture and subcritical crack growth in moist-air environments (both by stress-corrosion[17] and cyclic fatigue[16]) occurred predominantly along the interface in virtually every experiment; in fact, *in situ* fractures in an Auger spectroscopy unit revealed true interfacial separation with only SiO_2 on one fracture surface and metal on the other.[16] For samples bonded at 450°C, failure occurred at low G_c values, typically ~2 J/m^2, with stress-corrosion and fatigue thresholds as much as an order of magnitude lower, resulting in part from organic or other impurities at the interface; values exceeding 10 J/m^2, were obtained after bonding at higher temperatures.

Where cracks were deflected from the interface into the ceramic, it would be anticipated from considerations of the $K_{II} = 0$ path and the sign of the $\partial K_{II}/\partial c$ gradient (Fig. 4) that in the glass/Cu system, the crack should kink away from the interface as $\beta < 0$. This was in fact seen in experiments with both the DCB and bend geometries, where it appeared that the crack was drawn away from the interface by the modulus mismatch effect,* resulting in low G_c values. Conversely, with the Al_2O_3/metal systems where $\beta > 0$, cracks deviated from the interface are drawn back again, such that pieces of the ceramic are plucked out. This is illustrated for Al_2O_3/Cu interfaces by the metallographic crack-path section and fracture surfaces shown in Figs. 7 and 8, and is again consistent with the predictions in Fig. 4.

*In glass/metal DCB samples, cracks deviating from the interface generally broke off the glass arm of the specimen unless a side groove was used. However with this particular test-piece design, it is difficult to attribute this solely to modulus mismatch effects as the specimen geometry is inherently unstable to off-angle cracking.

A further demonstration of the prominent role of β in dictating whether cracks are drawn to, or deflected away from, the ceramic/metal interface is shown by results from the bend tests on glass/Cu ($\beta < 0$) and Al_2O_3/Al ($\beta > 0$) sandwich specimens, where notches placed in the ceramic

substrate initiated cracking at varying distances from the interface. Results showing the crack-path morphologies and corresponding micrographs are shown in Figs. 9 and 10, respectively. It is apparent that for the $Al_2O_3/Al/Al_2O_3$ samples, in accordance with the modulus mismatch predictions, the effect of the positive β is to draw cracks in the ceramic into the interface (Fig. 10a); in fact, cracks which initiate as far away as 5 times the metal-layer thickness are attracted to the metal layer (Fig. 9a). Where β is negative in the glass/Cu/glass specimens, conversely, cracks initiated in the glass at the interface and up to 3 metal-layer thicknesses away, all are deflected away from the metal layer (Fig. 9b, 10b).

Clearly, with "weak" interface systems, the crack trajectory is generally along the interface because the microstructural crack-path resistance is lower there; cracks in the ceramic will only find the interface if the compliance mismatch is such that $\beta > 0$.

(2) "Weak" Metal

Two examples where cracking in ceramic/metal/ceramic layered structures is confined to the metal layer were shown by Al_2O_3/Al bend and C(T) samples and by Al_2O_3/Al-4Mg C(T) samples *tested in cyclic fatigue;* both $\beta > 0$ systems. In these cases, the resulting toughness G_c depends primarily on the location of the crack (and its stability). For a crack within the metal layer, the linear-elastic analysis described above (Fig. 4), and that of Fleck *et al.*,[39] predicts a stable $K_{II} = 0$ path down the center if $\beta/|\alpha|$ exceeds a critical range, versus stable $K_{II} = 0$ paths near either interface if $\beta/|\alpha|$ is less, but positive, i.e., the darker hatched regime versus the unhatched regime in Fig. 4. Therefore, on the basis of α and β values of +0.686 and +0.143, respectively, for the Al_2O_3/Al systems, a centered crack within the metal layer is predicted. Contrary to these predictions, however, cracks in Al_2O_3/Al flexure samples propagated in the pure aluminum but well off the centerline within ~50 μm or so of the interface (Fig. 6). Similarly, in Al_2O_3/Al-4Mg C(T) samples, initial cyclic loading encouraged formation of a crack at the half-chevron pre-notch that soon ran near the interface, but ~5-20 μm into the metal (Fig. 11). Whereas these effects could be associated with easier initiation in the vicinity of the interface, it is

considered that the prime cause is associated with the inevitable presence of plasticity in the metal. Since crack-tip plasticity would have the effect of making the metal more compliant and incompressible, the observed cracking configurations would be anticipated simply by decreasing E_{Al} and increasing $\nu_{Al.} \rightarrow 0.5$. Crack paths near an interface would then be predicted since $\alpha \rightarrow 1$ and $\beta \rightarrow 0$; $2E_{Al}/3$ and the self-consistent $\nu_{Al} \sim 0.4$ are sufficient.

(3) "Weak" Ceramic

Where the ceramic provides the weaker microstructural crack path, cracking predominates in this phase and the crack path generally conforms to the linear-elastic predictions of Fig. 4. For example, as described above, the modulus mismatch acts to drive cracks away from the metal layer into the ceramic where $\beta < 0$, i.e., in glass/Cu sandwich samples (Fig. 10b), resulting in a low toughness of the joint. Where $\beta > 0$, cracks are conversely attracted to the metal layer and tend to pluck out pieces of the ceramic. Such behavior was shown by Al_2O_3/Al-4Mg C(T) samples under monotonic loading, and sometimes by Al_2O_3/Au and Al_2O_3/Pt bend samples (Figs. 12 and 13). In fact, in the positive β systems, cracks are drawn away from the weaker microstructural path in the ceramic to the stronger interface and metal, and can often blunt out in the metal phase with resulting high toughness. This is clearly shown for Al_2O_3/Al-4Mg joints in Fig. 13, where a large contribution to the high G_c value is apparent from extensive plasticity associated with blunting in the metal layer. In these cases, the mutually opposing influence on the crack path of the lowest microstructural resistance and highest crack-tip driving force (due to far-field loading and modulus mismatch effects) generally results in complex cracking configurations (e.g., Fig. 12) with high yet erratic toughness values.

(4) Role of Residual Stress

For most diffusion-bonded samples, the thermal expansion mismatch leads to in-plane residual tensile stresses in the metal layer, σ_{xx}^{res}, which are at the yield point after bonding and cooling, viz.:

$$(\alpha_m - \alpha_c)(T_b - T_{rt}) > \sigma_y / E_2 \cong \sigma_{xx}^{res} / E_2 , \qquad (17)$$

where α_m and α_c are the thermal expansion coefficients of the metal and ceramic layers, respectively, T_b is the bonding temperature and T_{rt} is room temperature. Yield stresses for the metals studied have been estimated from microhardness measurements as 1/3 of the hardness for the thicker metal layers and from residual stresses deduced from X-ray diffraction measurements on thin evaporated layers.[48] As listed in ref. 42, the yield stresses range from ~70 to 230 MPa in the thicker layers of metals (bonded near or above their melting points) to ~200 to 350 MPa in the evaporated copper layers.

The presence of such thermally induced residual tensile stresses in the metal layer means that the local T-stress in the present experiments will be positive (Eq. 7), regardless of specimen geometry. Following Cotterell and Rice's linear-elastic crack-deflection analysis,[36] a straight crack propagating along a $K_{II} = 0$ path is only directionally stable if $T < 0$; a positive T-stress should cause the crack to veer off from a straight trajectory if perturbed by some microstructural inhomogeneity. This suggests that in the Al_2O_3/metal/Al_2O_3 sandwich structures where cracking proceeds in the metal layer, a wavy fracture trajectory should result.[39] Whereas there was much evidence of crack jumping between interfaces (see next section), wavy crack profiles were rarely observed under monotonic loading. They were not totally non-existent, however; Fig. 14, for example, shows such a profile in Al_2O_3/Cu although the origin of the crack meandering in this instance is probably more associated with specific microstructural features in the metal layer rather than instability induced by a positive T-stress.

The absence of unstable crack paths in the present tests almost certainly results from the presence of extensive plasticity within the metal layer, which effectively relieves the residual stresses. The more extensive plasticity is evident from slip lines on the metal (Figs. 11, 12 and 13) and by crack blunting of arrested cracks at Al_2O_3/Al-Mg interfaces (Fig. 13); scanning electron microscopy and electron-channeling studies for Al_2O_3/Nb also have clearly shown this effect.[48]

The notion of plasticity within the layer inhibiting unstable crack path is further supported by observations that, unlike in G_c tests, fatigue-crack growth profiles in the metal are more often wavy in trajectory. Since fatigue cracks grow in these systems at G levels some 4 to 10 times smaller than G_c,[16,42] the associated crack-tip plastic-zone sizes are far smaller.

To quantitatively assess the extent of plasticity in the layer, the approximate height of the crack-tip plastic zones in the metal, r_y, expected under pure mode I loading are calculated in Table II (assuming the metal layers were thick enough not to limit the zone) by modifying simple expressions for homogeneous materials, consistent with Eq. (1); this gives:[42]

$$r_y = G_c E_1' E_2' / \pi \sigma_y^2 \left(E_1' + E_2' \right), \tag{18}$$

where σ_y is the yield stress.[49] These estimates span four orders of magnitude and, in the case of glass/Cu samples, have been corroborated by X-ray diffraction and transmission electron microscopy observations.[50] The "unconstrained" plastic-zone heights vary from being trivial in size to significantly exceeding the metal-layer thicknesses used; correspondingly, in several instances, the extent of plasticity was clearly constrained by the metal thickness.

(5) Crack Jumping

As described above, initial crack propagation in many of the Al_2O_3/metal samples occurred close to the interface but not at it; however, subsequent crack propagation often involved far more complex cracking configurations. For example, during initial advance in Al_2O_3/Al-Mg compact samples, cyclic fatigue cracks were observed to grow in the metal layer close to one of the interfaces yet under subsequent monotonic loading, crack growth usually switched to the ceramic, often after crack re-initiation on the opposite side of the sandwiched metal layer (Fig. 12). Moreover, this process was invariably accompanied by extensive plasticity causing significant crack-tip blunting, with associated slip lines radiating out from the blunted crack tip across the metal film (Figs. 11 and 13). Such crack jumping from interface to interface has the effect of creating metal-layer bridges across the crack surfaces (Fig. 15); the resulting crack-tip shielding

from crack bridging, and accompanying plasticity and blunting, can lead to very high toughness values. This was apparent in resistance-curve fracture toughness tests on Al_2O_3/Al-Mg samples, where during the period wherein the re-nucleation events occurred and the intervening metal ligament tore, the G_c toughness rose to about 400 J/m^2, well above that of the ceramic (~20-100 J/m^2), yet small compared to the alloy toughness, ~10^4 J/m^2. Another example[21] of crack jumping across the metal layer is apparent in glass/Cu DCB tests with ~2 μm Cu films; here both interfaces alternately crack, although only when nominally similar, yielding high G_c values of ~5 J/m^2.

The tendency to re-initiate fracture across the metal layer seen in Al_2O_3/Al-Mg and certain glass/Cu structures, or on further loading in flexure of arrested cracks (e.g., Fig. 13a), is reminiscent of behavior found over a wide range of thickness in several systems which fail primarily at the interface. Mechanistically, this could result from crack blunting, which reduces the stresses near the main crack tip to a small multiple of the metal's yield stress, such that the stresses on the far interface are sufficient to trigger the requisite damage (owing to variations in the near-interfacial strength due to heterogeneous impurities or residual porosity). However, it is also apparent that crack jumping occurs more readily when plasticity spans the entire metal layer. In all the instances of severe crack jumping observed, the computed plastic-zone size, r_y, was comparable to the layer thickness. For example, crack jumping was seen in 4-point flexure tests on Al_2O_3/Au sandwich specimens made from 25-100 μm metal foils, but was absent in specimens with thicker metal layers.[25] These observations strongly suggest that slip-band intersections with the ceramic play a key role in promoting this phenomenon.

VI. Discussion

The various ceramic/metal interfaces assessed here differ widely regarding metal thickness, the properties of adjoining materials, and the fracture resistances. Moreover, the crack-path responses are exceedingly varied (Figs. 10-15). Sometimes a fatigue pre-crack rather easily enters the ceramic perhaps expedited by flaws from processing or the cyclic loading. Often instead, a

fatigue crack blunts further, and damage formed near the interface across the layer creates a new crack. Similarly, upon overloading a pre-notch in the metal without a fatigue crack, a crack initiated near an interface will become well established within the ceramic before the intervening metal ligament cracks or tears. Furthermore, after appreciable advance, the crack may stall and again jump across the layer, e.g., Fig. 15. The metallic deformation attending such transitions requires high loads prior to eventually, if ever, attaining an unbridged crack on one side of the metal, yielding steeply rising and then falling resistance curves.[16] Once in the ceramic, the crack presumably follows a $K_{II} = 0$ path, balancing the $\beta > 0$ attraction to the layer, the instability of an off-centered crack, and any bridging forces.

With respect to the toughness of ceramic/metal joints, with all the ceramic/metal couples examined, plasticity within the metal likely constitutes most of the fracture energy, even in the glass/Cu samples. In addition, it is clear that the nature of the crack path and its selection of a particular phase has an important bearing on the value of G_c. In particular, where the crack path with the lowest microstructural resistance is distinctly different from that offering highest crack-tip driving force (due to far-field loading and modulus mismatch effects), the resulting complex cracking configurations, including crack jumping between interfaces with resulting crack blunting and metal-layer bridging, provide potent contributions to the toughness. To predict these effects *a priori*, knowledge of the modulus mismatch parameters between the metal and the ceramic, and specifically of the sign of β, is critical, together with an understanding of the microstructurally "weak" paths. However, for certain of the linear-elastic predictions of crack trajectory, based on the location of the $K_{II} = 0$ path and the sign of the T (or residual) stress and the gradient $\partial K_{II}/\partial c$, allowance clearly must be made for the presence of plasticity within the metal layer.

Finally, additional to the phase angle of the global and local fields, the type of loading is important in dictating the crack path. In Al_2O_3/Al-Mg samples, for example, the crack preferred the ceramic rather than the interface under monotonic loading but extended within the metal under cyclic loading, somewhat analogous to the relationship depicted in Fig. 5b. However, in this instance, fatigue loading, rather than a direct reduction in yield stress, has created a situation

wherein the crack-tip stresses are insufficient to cause crack extension within the ceramic, despite the fact that more than thrice the energy is dissipated cracking the metal than had the crack been isolated within the ceramic.

VII. Conclusions

Based on a theoretical and experimental study of the trajectory of crack paths *at* or *near* interfaces, and the resulting toughness, in a series of ceramic/metal/ceramic sandwich structures, involving glass/Cu, SiO_2/Cu, Al_2O_3/Al-4Mg, Al_2O_3/Au, Al_2O_3/Cu and Al_2O_3/Pt systems, the following conclusions can be made:

1. Linear-elastic driving force calculations project that cracks will follow a path where $K_{II} = 0$ (essentially equivalent to where G is maximum). Accordingly, for cracks *at* an interface where the far-field loading is mode I, cracks will kink away from the metal layer for bimaterial couples where the second Dundurs' parameter $\beta = 0$, irrespective of the value of first Dundurs' parameter α; conversely, where $\alpha = 0$, cracks will kink into the metal layer for $\beta > 0$ and away from the layer if $\beta < 0$.

2. Correspondingly, for cracks *near* interfaces in sandwich structures, linear-elastic projections imply that cracks will follow a straight parallel path if $K_{II} = 0$ and $\partial K_{II}/\partial c > 0$. For mode I far-field loading, however, three regimes of cracking configurations exist depending upon the value and sign of α and β.

3. Some, but not all, key trends for crack trajectory, and by implication for the pertinent fracture resistance, match the linear-elastic predictions for modulus mismatch effects; however, often the plastic zones in the metal are too large relative to layer thickness to confidently use computations based on elastic stress fields to deduce crack kinking tendencies.

4. At "weak" interfaces, the crack generally stays at the interface; near such interfaces, the crack will be drawn into the interface only if the compliance mismatch is such that β is positive. Where the metal provides the "weak" path, cracks are drawn to the metal layer where $\beta > 0$, and deflected from the weak path where $\beta < 0$; here the toughness G_c depends on the location and stability of the crack. However, where $\beta > 0$, the location of the crack path within the metal layer does not match prediction, primarily because of plasticity within the layer. Where the ceramic provides the "weak" path, cracks deflect away from the metal layer and remain in the ceramic where $\beta < 0$. Where $\beta > 0$, conversely, cracks are drawn from the weak path to the "stronger" interface and metal; cracking configurations in this case can become complex resulting in very high, but erratic, toughness values.

5. In most ceramic/metal/ceramic sandwich tests, with metal-layer thicknesses spanning three orders of magnitude, crack jumping across the layer or cracking on two interfaces was apparent where computations of the unconstrained crack-tip plastic-zone size exceeded the layer thickness, and was absent where the plastic zone was much smaller. This suggests that fracture re-initiation owing to incompatibility at the plastic-zone/ceramic boundary is important; the resulting bridging by metal ligaments was found to markedly increase crack-growth resistance in these samples.

6. Crack meandering within the metal layer, which is promoted by a positive T-stress, was rarely seen, despite the presence of processing-induced tensile residual stresses. The lack of an effect of the T-stress on de-stabilizing the crack path was attributed to the extensive plasticity within the metal layer.

Acknowledgments: This work was supported by the Director, Office of Energy Research, Office of Basic Energy Sciences, Materials Sciences Division of the U.S. Department of Energy under Contract No. DE-AC03-76SF00098.

References

1. A. G. Evans, "The Mechanical Properties of Reinforced Ceramic, Metal and Intermetallic Matrix Composites", pp. 3-32 in *Fatigue of Advanced Materials*, Edited by R. O. Ritchie, R. H. Dauskardt, and B. N. Cox, MCEP Publishing Ltd., Edgbaston, U.K., 1991.

2. R. R. Tummala, and E. J. Rymaszewski, "Microelectronic Packaging Handbook", Van Nostrand Reinhold, New York, NY, 1989.

3. D. E. Pitkanen, and C. J. Speerschneider, "Environmental Effects on Copper Thick Film Microcircuits", *IEEE Trans.*, **CHMT-4** [3], 250-56 (1981).

4. J. Uebbing, "Mechanisms of Temperature Cycle Fatigue in Encapsulated Optoelectronic Devices", pp. 149-56 in *Proceedings of 19th Annual International Reliability Physics Symposium, IEEE,* 1981.

5. F. F. Oettinger, "Thermal Evaluation of VLSI Packages using Test Chips - A Critical Review", *Solid State Tech.*, **27** [2], 169-79 (1984).

6. D. P. Seraphim, R. C. Lasky, and C.Y. Li, "Principles of Electronic Packaging", McGraw-Hill, New York, NY, 1989 .

7. F. N. Sinnadurai, Editor, "Handbook of Microelectronics Packaging and Interconnection Technologies", Electrochemical Publications Ltd., Anchor Press, 1985.

8. S. Suresh, and A. Needleman, Editors, "Interfacial Phenomena in Composites: Processing, Characterization, and Mechanical Properties", *Mater. Sci. Eng.*, **A107** [1-2], (1989).

9. M. Rühle, A. G. Evans, M. F. Ashby, and J. P. Hirth, Editors, "Metal-Ceramic Interfaces", Acta-Scripta Metallurgica Proceedings Series 4, Pergamon Press, Oxford, U.K. 1990.

10. B. J. Dalgleish, M. C. Lu, and A. G. Evans, "The Strength of Ceramics Bonded with Metals", *Acta Metall.*, **36** [8], 2029-35 (1988).

11. H. C. Cao, M. D. Thouless, and A. G. Evans, "Residual Stresses and Cracking in Brittle Solids Bonded with a Thin Ductile Layer", *Acta Metall.*, **36** [8], 2037-46 (1988).

12. B. J. Dalgleish, K. P. Trumble, and A. G. Evans, "The Strength and Fracture of Alumina Bonded with Aluminum Alloys", *Acta Metall.*, **36** [7], 1923-31 (1989).

13. A. G. Evans, M. Rühle, B. J. Dalgleish, and P. G. Charalambides, "The Fracture Energy of Bimaterial Interfaces", pp. 345-364 in *Metal-Ceramic Interfaces*, Edited by M. Rühle, A. G. Evans, M. F. Ashby, and J. P. Hirth, Pergamon Press, Oxford, U.K., 1990.

14. T. S. Oh, R. M. Cannon, J. Rödel, A. M. Glaeser, and R. O. Ritchie, "Effects of Near Interfacial Microstructures on Toughness and Subcritical Crack Growth in Ceramic/Metal Systems", pp. 567-581 in *Interfaces in Polymers, Ceramics and Metal-Matrix Composites*, Edited by H. Ishida, Elsevier Science, New York, NY, 1988.

15. J. T. Klomp, "Ceramic-Metal Interactions", pp. 381-391 in *Electronic Packaging Materials Science,* Proceedinds of Materials Research Society Symposium, Vol. 40, Edited by E.A. Giess, K.-N. Tu, and D. R. Uhlmann, Materials Research Society, Pittsburgh, PA, 1985.

16. R. M. Cannon, B. J. Dalgleish, R. H. Dauskardt, T. S. Oh, and R. O. Ritchie, "Cyclic Fatigue-Crack Propagation along Ceramic/Metal Interfaces", *Acta. Metall. Mater.*, **39** [9], 2145-56 (1991).

17. T. S. Oh, R. M. Cannon, and R. O. Ritchie, "Subcritical Crack Growth along Ceramic-Metal Interfaces", *J. Am. Ceram. Soc.*, **70** [12], C353-55 (1987).

18. P. F. Becher, and W. L. Newell, "Adherence-Fracture Energy of a Glass-Bonded Thick-Film Conductor: Effect of Firing Conditions", *J. Mat. Sci.*, **12**, 90-96 (1977).

19. J. J. Mecholsky, "A Chevron-Notched Specimen for Fracture Toughness Measurements of Ceramic-Metal Interfaces", pp. 324-336 in *ASTM STP* 855, American Society for Testing and Materials, Philadelphia, PA, 1985.

20. R. M. Cannon, V. Jayaram, B. J. Dalgleish, and R. M. Fisher, "Microstructural and Chemical Components of Ceramic-Metal Interface Fracture Energies", pp. 121-126 in *Electronic Packaging Materials Science II,* Proceedings of Materials Research Society Symposium, Vol. 72, Edited by K. A. Jackson, R. C. Pohanka, D. R. Uhlmann, and D. R. Ulrich, Materials Research Society, Pittsburgh, PA, 1986.

21. R. M. Cannon, V. Jayaram, B. J. Dalgleish, and R. M. Fisher, "Fracture Energies of Ceramic-Metal Interfaces", pp. 959-968 in *Ceramic Microstructures '86: Role of Interfaces*, Edited by J. A. Pask and A. G. Evans, Plenum Press, New York, NY, 1987.

22. T. S. Oh, J. Rödel, R. M. Cannon, and R. O. Ritchie, "Ceramic/Metal Interfacial Crack Growth: Toughening by Controlled Microcracks and Interfacial Geometries", *Acta Metall,* **36** [6], 2083-93 (1988).

23. I. E. Reimanis, B. J. Dalgleish, M. Brahy, M. Rühle, and A. G. Evans, "Effects of Plasticity on the Crack Propagation Resistance of a Metal/Ceramic Interface", *Acta Metall. Mater.*, **38** [12], 2645-52 (1990).

24. H. F. Fischmeister, G. Elssner, B. Gibbesch, and W. Mader, "Preparation, Properties and Structure of Metal/Oxide Interfaces", pp. 227-38 in *Metal-Ceramic Joints*, Proceedings of Materials Research Society International Meeting on Advanced Materials, Vol. 8, Materials Research Society, Pittsburgh, PA, 1989.

25. M. Turwitt, G. Elssner, and G. Petzow, "On the Fracture Behavior and Microstructure of Metal-to-Ceramic Joints", pp. 969-979 in *Ceramic Microstructures '86, Role of Interfaces,* Edited by J. A. Pask and A. G. Evans, Plenum Press, New York, NY, 1987.

26. J. R. Rice, "Elastic Fracture Concepts for Interfacial Cracks", *J. Appl. Mech.*, **55** [1], 98-103 (1988).

27. J. R. Rice, Z. Suo, and J.-S. Wang, "Mechanics and Thermodynamics of Brittle Interfacial Failure in Bimaterial Systems," pp. 269-294 in *Metal-Ceramic Interfaces*, Edited by M. Rühle, A. G. Evans, M. F. Ashby, and J. P. Hirth, Pergamon Press, Oxford, U.K., 1990.

28. J. W. Hutchinson, M. E. Mear, and J. R. Rice, "Crack Paralleling an Interface between Dissimilar Materials", *J. Appl. Mech.*, **54**, 828-32 (1987).

29. J. W. Hutchinson and Z. Suo, "Mixed Mode Cracking in Layered Materials", *Adv. Appl. Mech.*, **29**, 63-187 (1991).

30. C. F. Shih and R. J. Asaro, "Elastic-Plastic Analysis of Cracks on Bimaterial Interfaces: Part 1 - Small Scale Yielding", *J. Appl. Mech.*, **55**, 299-316 (1988).

31. J. J. Dundurs, "Edge-Bonded Dissimilar Orthogonal Elastic Wedges under Normal and Shear Loading" *J. Appl. Mech.*, **36**, 650-52 (1969).

32. T. Suga, G. Elssner, and S. Schmauder, "Composite Parameters and Mechanical Compatibility of Material Joints", *J. Composite Matls.*, **22**, 917-34 (1989).

33. Z. Suo and J. W. Hutchinson, "Sandwich Specimens for Measuring Interface Crack Toughness", *Mater. Sci. Eng.*, **A107**, 135-43 (1989).

34. Z. Suo and J. W. Hutchinson, "Steady-State Cracking in Brittle Substrate Beneath Adherent Films," *Int. J. Solids Structures*, **25**, 1337-53 (1989).

35. S. G. Larsson and A. J. Carlsson, "Influence of Non-Singular Stress Terms and Specimen Geometry on Small-Scale Yielding at Crack Tips in Elastic-Plastic Materials", *J. Mech. Phys. Solids*, **21**, 263-77 (1973).

36. B. Cotterell and J. W. Rice, "Slightly Curved or Kinked Cracks", *Int. J. Fract. Mech.*, **16** [2], 155-69 (1980).

37. G. Dreier, S. Schmauder, and M. Meyer, "T-Stress Due to Thermal Residual Stresses in Bimaterials with Isotropic, Linear Elastic Composites," *Eng. Fract. Mech.*, **35** (1992), in press.

38. S. Schmauder and M. Meyer, "Influence of Thermal Residual Stresses on the Interface Crack," pp. 149-174 in *Finite Elements in Engineering Applications*, INTES GmbH, Stuttgart, Germany, 1992.

39. N. A. Fleck, J. W. Hutchinson, and Z. Suo, "Crack Path Selection in a Brittle Adhesive Layer", *Int. J. Solids Structures*, **27** [13], 1683-703 (1991).

40. M.-Y. He and Hutchinson, "Kinking of Crack out of an Interface", *J. Appl. Mech.*, **56** [2], 270-78 (1989).

41. C. F. Shih, R. J. Asaro, and N. P. O'Dowd, "Cracks on Bimaterial Interfaces: Plasticity Aspects", pp. 313-325 in *Metal-Ceramic Interfaces,* Edited by M. Rühle, A. G. Evans, M. F. Ashby, and J. P. Hirth, Pergamon Press, Oxford, U. K. 1990.

42. R. M. Cannon, B. J. Dalgleish, R. H. Dauskardt, R. M. Fisher, T. S. Oh, and R. O. Ritchie, "Ceramic-Metal Interfaces: Monotonic and Cyclic Fracture Resistance", pp. 459-482 in *Fatigue of Advanced Materials* Edited by R. O. Ritchie, R. H. Dauskardt, and B. N. Cox, MCEP Publishing Ltd., Edgbaston, U.K. 1991.

43. T. S. Oh, R. M. Cannon, and R. O. Ritchie, "Tailored Microstructures to Control Interfacial Toughness", pp. 219-24 in *Thin Films: Stresses and Mechanical Properties,* Proceedings of Materials Research Society Symposium, Vol. 130, Edited by J. C. Bravman, W. D. Nix, D. M. Barnett, and D. A. Smith, Materials Research Society, Pittsburgh, PA, 1989.

44. R. H. Dauskardt and R. O. Ritchie, "Cyclic Fatigue-Crack Growth Behavior in Ceramics", *Closed Loop*, 17 [2], 7-17 (1989).

45. S. M. Wiederhorn, A. M. Shorband, and R. L. Moses, "Critical Analysis of the Theory of the Double Cantilever Method for Measuring Fracture Surface Energy", *J. Appl. Phys.*, 9 [3], 1569-72 (1968).

46. H. Tada, P. C. Paris, and G. R. Irwin, "Stress Analysis of Cracks Handbook", Paris Publications Inc./Del Research Corp., St. Louis, MO, 1985.

47. A. G. Evans, B. J. Dalgleish, M.-Y. He, and J. W. Hutchinson, "On Crack Path Selection and the Interfacial Fracture Energy in Bimaterial Systems", *Acta Metall.*, 37 [12], 3249-54 (1989).

48. M. Rühle, private communication, Max-Planck Institute, Stuttgart, Germany, 1991.

49. C. F. Shih, "Relationship between the J-Integral and the Crack Opening Displacement for Stationary and Extending Cracks", *J. Mech. Phys. Solids*, 29, 305-30 (1981).

50. A. G. Fox and R. M. Cannon, "X-Ray Diffraction and TEM Studies of the Delamination of Copper Thin Films from Glass and Silica Substrates", pp. 329-334 in *Proceedings of Materials Research Society Symposium,* Vol. 167, Materials Research Society, Pittsburgh, PA, 1990.

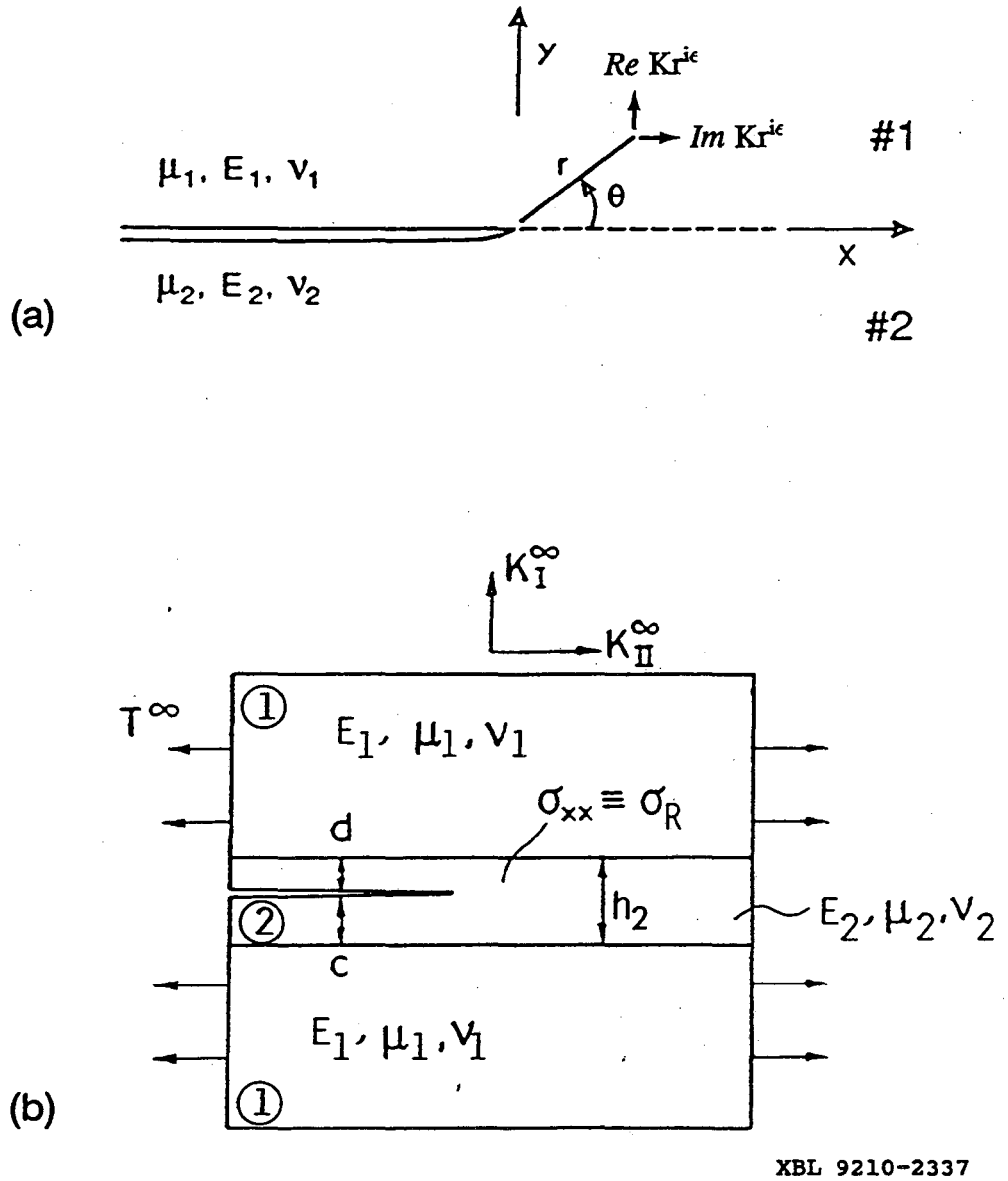

Figure 1: Conventions for crack tip a) *at* interface between two linear-elastic materials #1 and #2, with shear modulus μ_i, Young's modulus E_i and Poisson's ratio ν_i, and b) near interface in layered specimen of material #2 sandwiched between material #1.

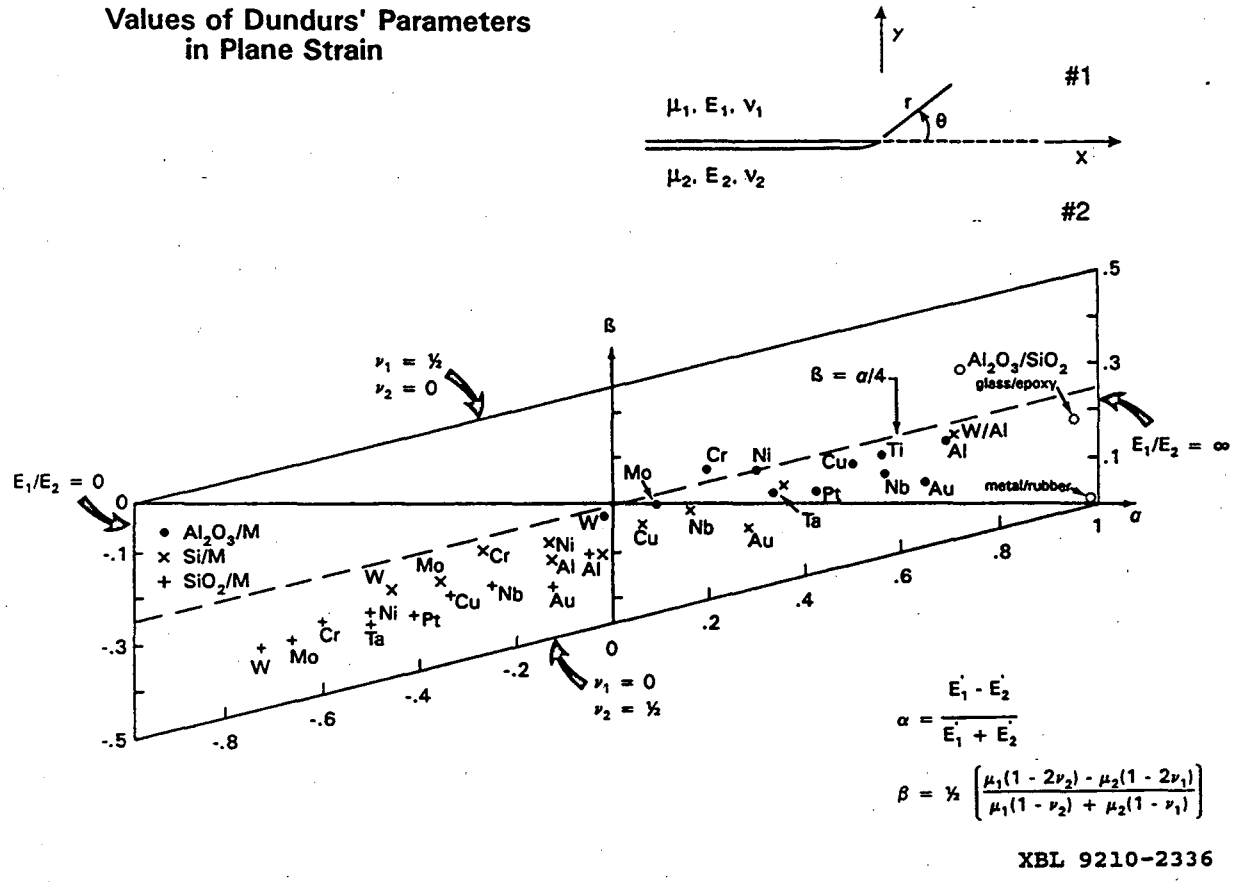

Figure 2: Plot of the elastic mismatch (Dundurs') parameters α and β in plane strain for a variety of bimaterial couples, showing alumina/metal, silicon/metal, and silica/metal interfaces.

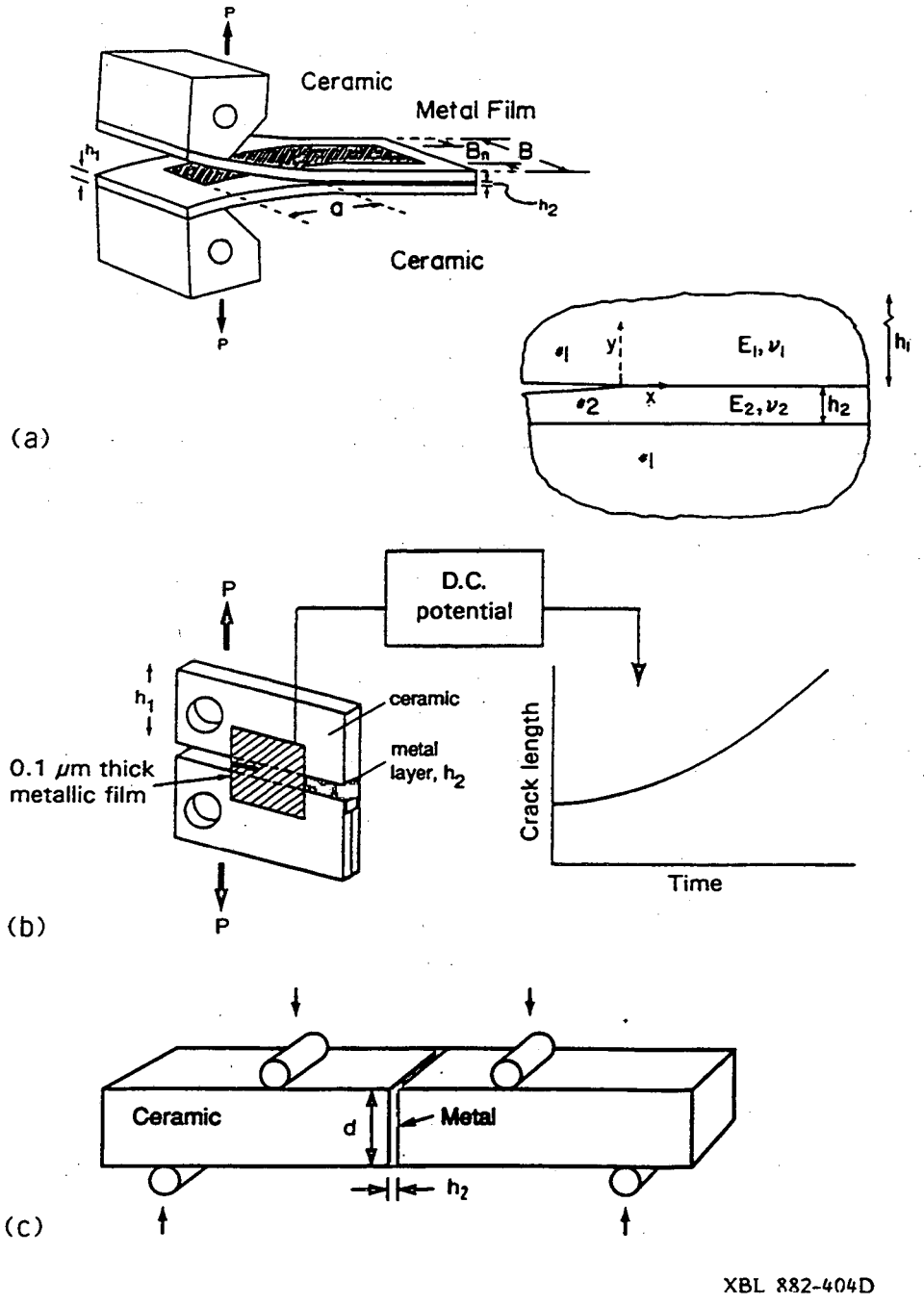

Figure 3: Geometries used to test metal/ceramic sandwich samples under far-field mode I conditions, showing a) double-cantilever bend - DCB, b) compact tension - C(T), and 4-point bend (flexure) specimens. Compact geometry in b) additionally shows schematic of the electrical-potential technique used to monitor crack length.

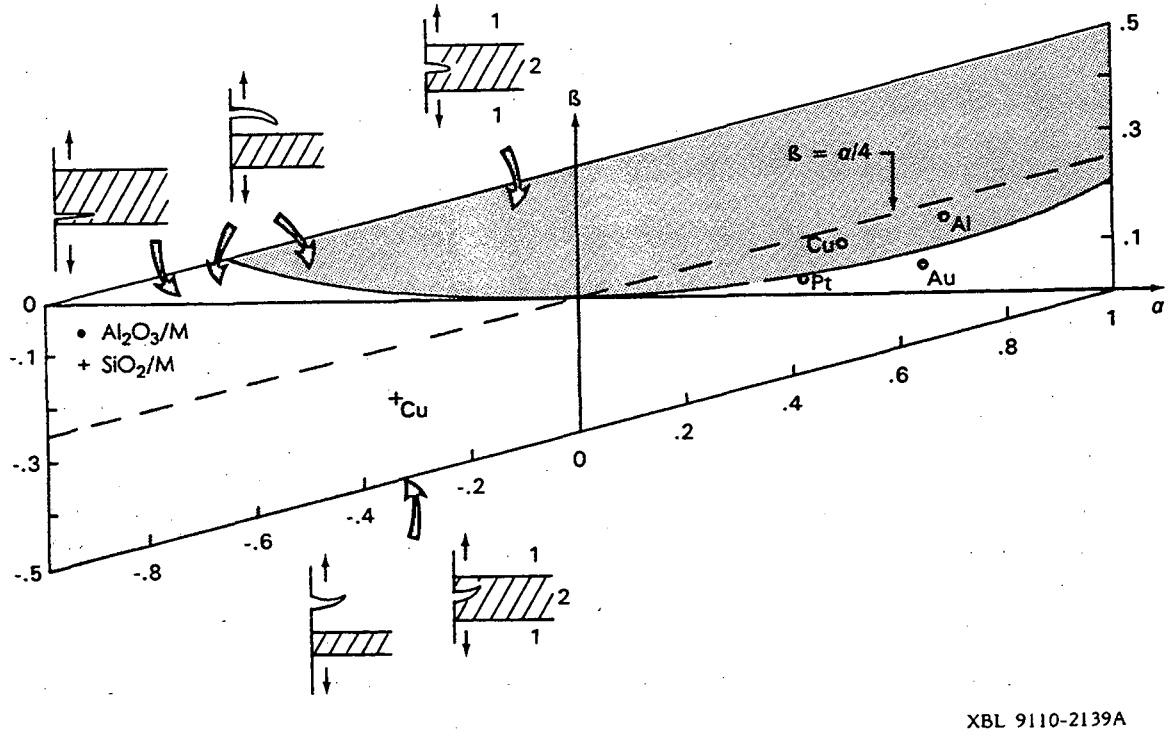

XBL 9110-2139A

Figure 4: Plot of the elastic mismatch (Dundurs') parameters α and β in plane strain, showing three predicted regimes of crack-path trajectories with $K_{II} = 0$ for ceramic/metal sandwich geometries subjected to far-field mode I loading.

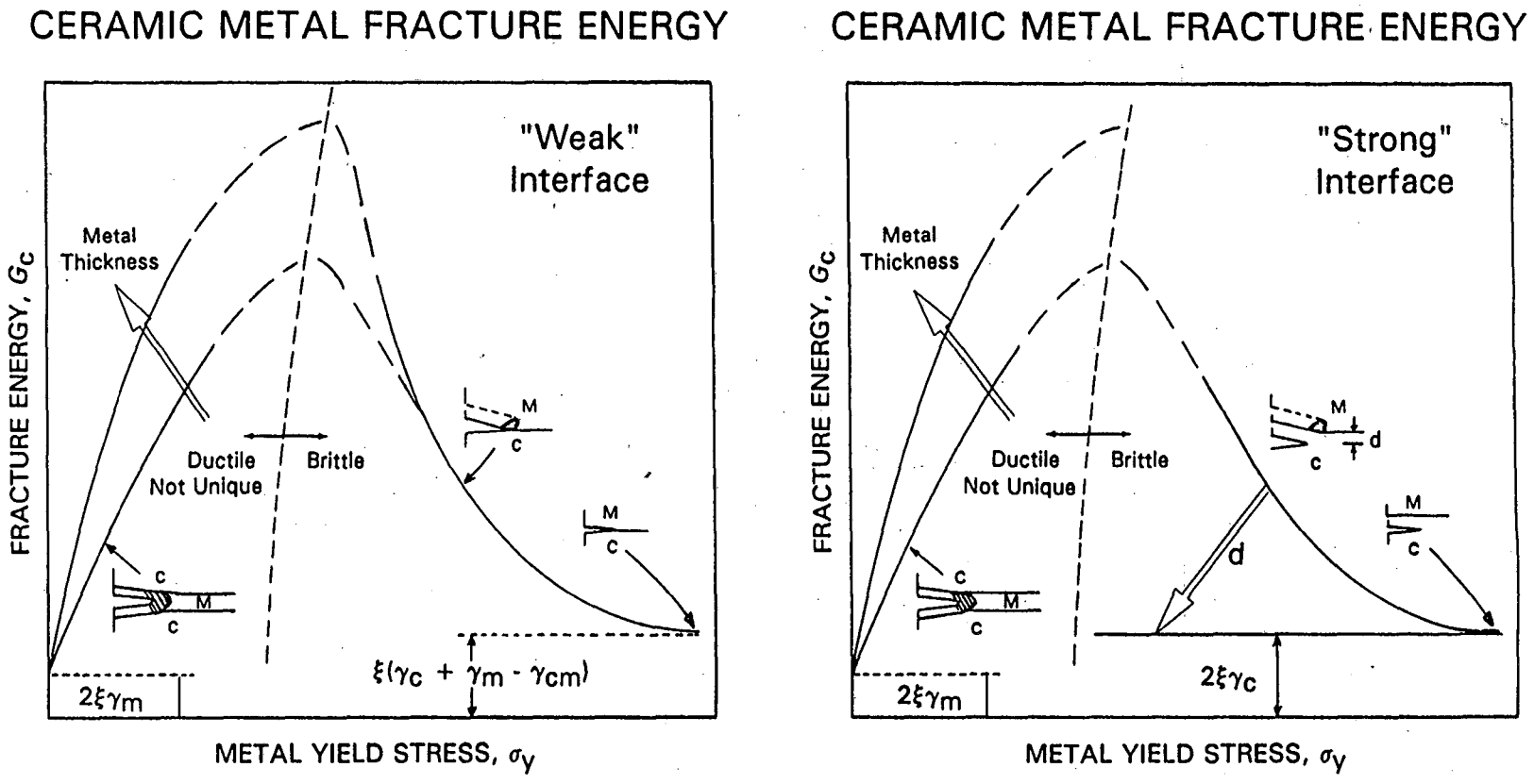

Figure 5: Expected interrelations among interfacial bond strength, metal yield stress, fracture energy and crack path for ceramic/metal interfaces or ceramic/metal/ceramic (C/M/C) sandwich samples.

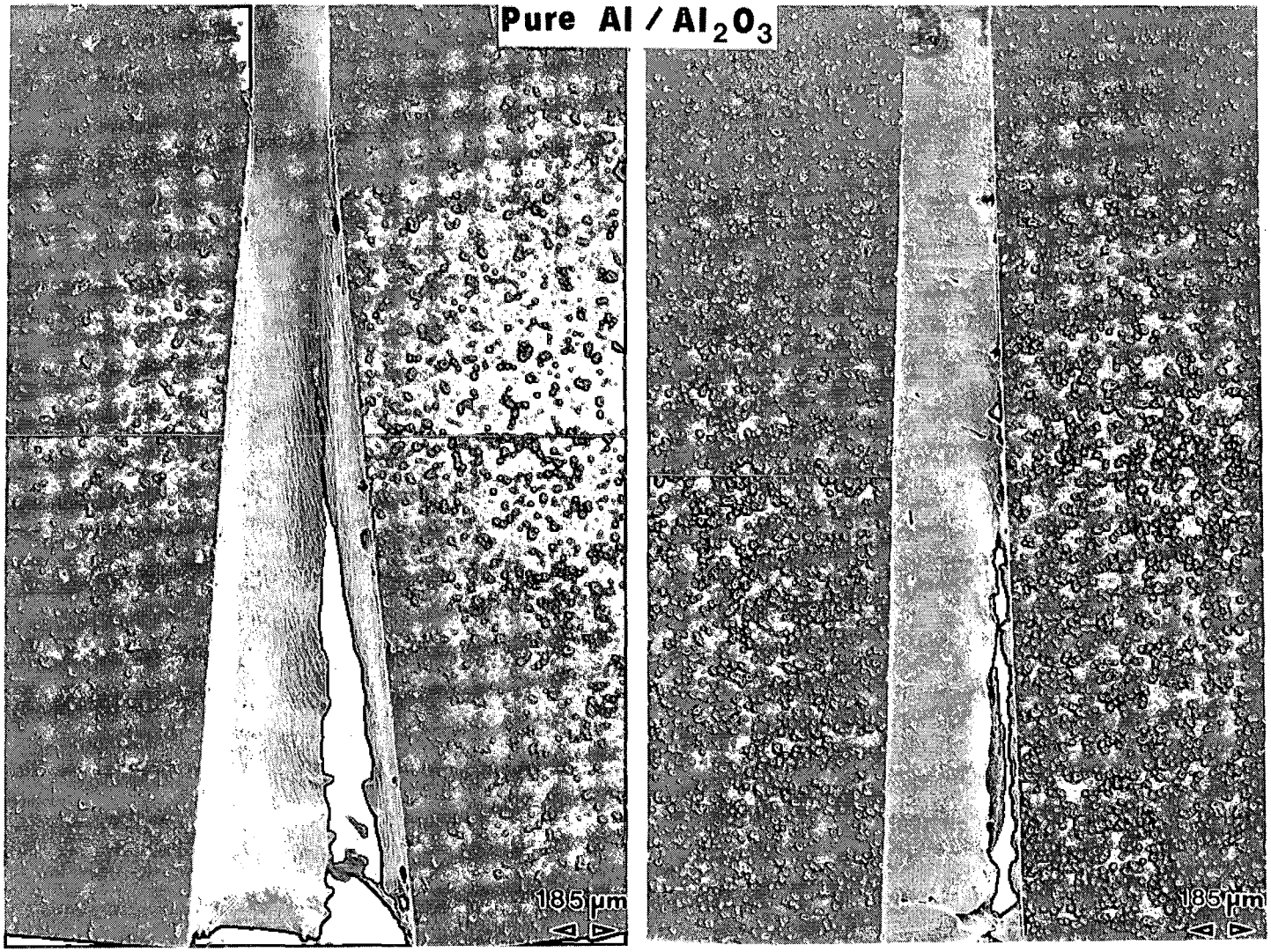

XBB 916-4542

Figure 6: Scanning electron images of sides of Al_2O_3/pureAl/Al_2O_3 ($\beta > 0$) 4-point bend sandwich samples, showing two examples of failure in the pure aluminum. Note that cracking in the metal layer proceeds near the interface and not along the centerline.

Al_2O_3/Cu

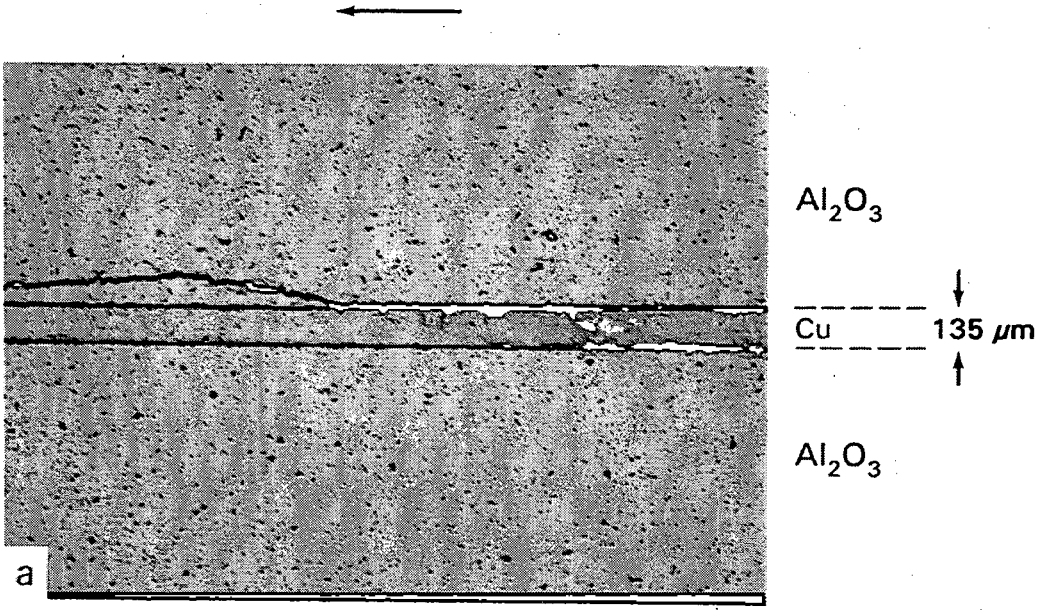

XBB 916-4854 (Top)

Figure 7: Scanning electron image of crack path in $Al_2O_3/Cu/Al_2O_3$ ($\beta > 0$) 4-point bend sandwich sample, showing predominantly interfacial failure with deflected cracks being drawn back to the interface. This cracking morphology effectively "plucks" pieces out of the ceramic.

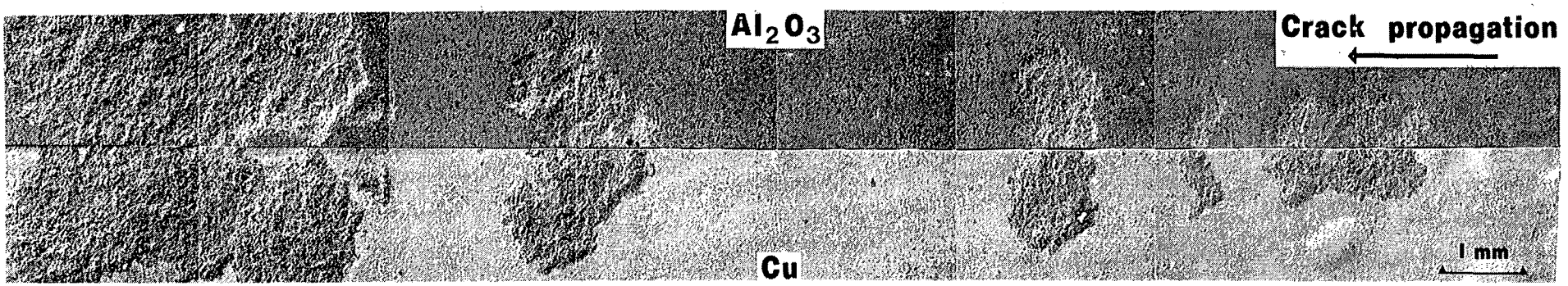

XBB 916-4540

Figure 8: Scanning electron image of fracture surfaces in $Al_2O_3/Cu/Al_2O_3$ ($\beta > 0$) 4-point bend sandwich sample corresponding to Figure 7, showing predominantly interfacial failure with deflected cracks "plucking" out pieces of the ceramic.

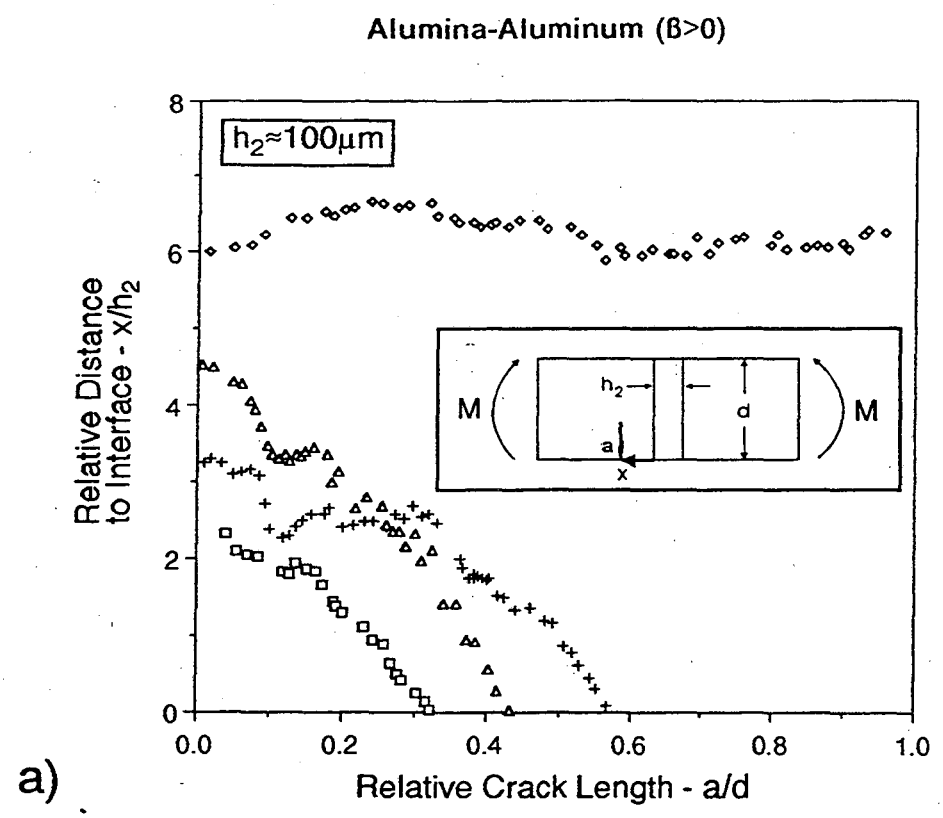

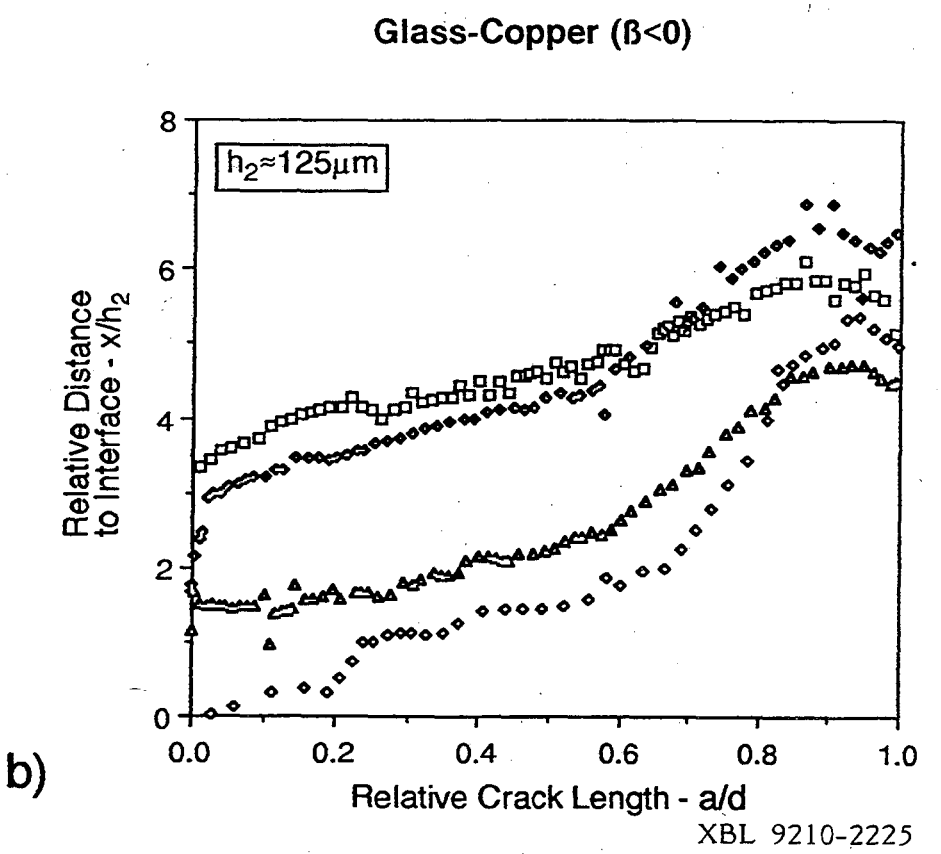

Figure 9: Plots of the location and path of cracks initiated in the ceramic substrate of ceramic/metal sandwich 4-point bend specimens at varying distances from the interfaces, showing cracks a) being drawn to the metal layer with Al_2O_3/Cu ($\beta > 0$), and b) deflected away from the layer in glass/Cu ($\beta < 0$).

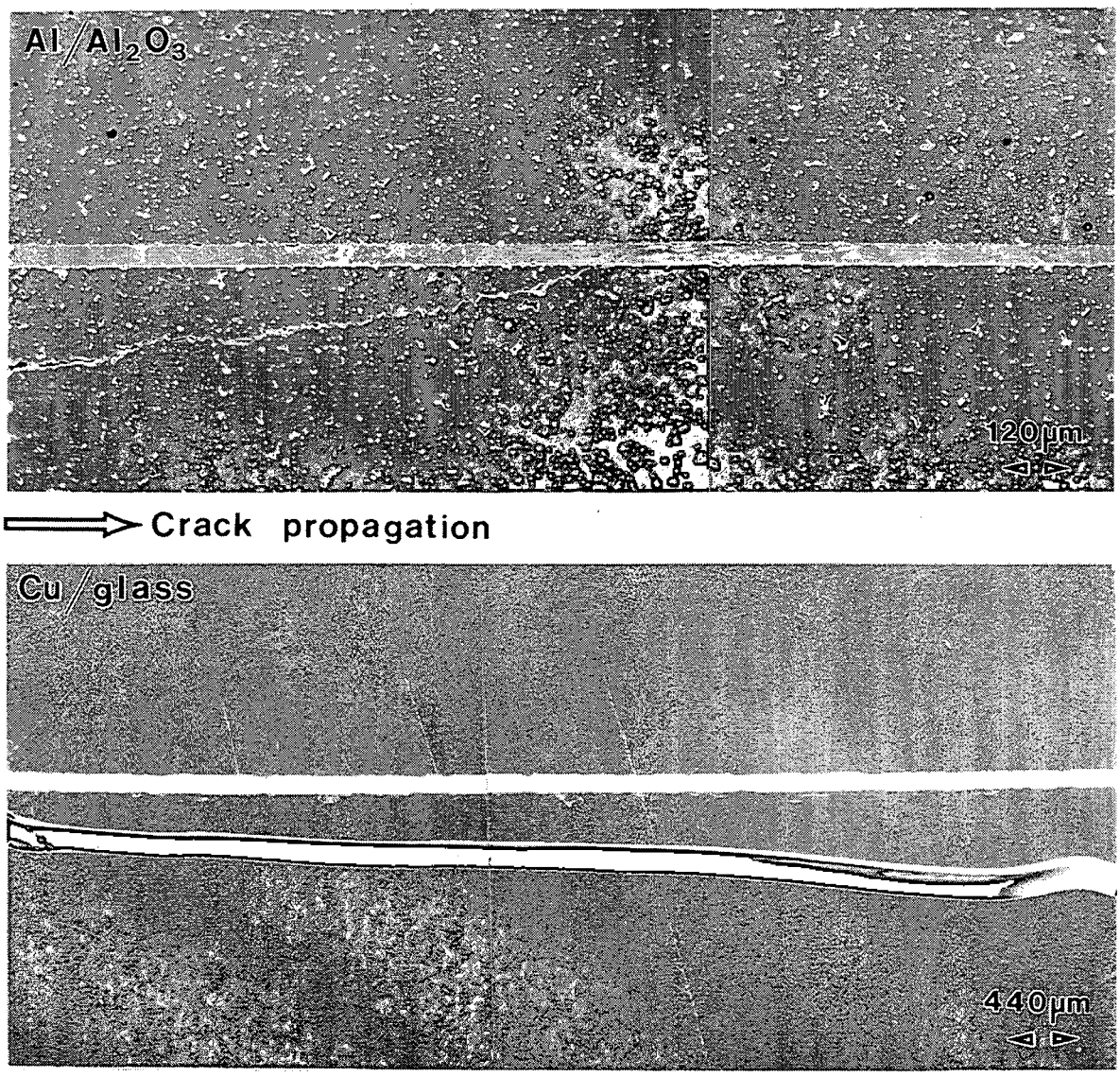

Figure 10: Scanning electron micrographs of the crack-path profiles corresponding to Figure 9, showing cracks a) being drawn to the metal layer with Al_2O_3/Cu ($\beta > 0$), and b) deflected away from the layer in glass/Cu ($\beta < 0$).

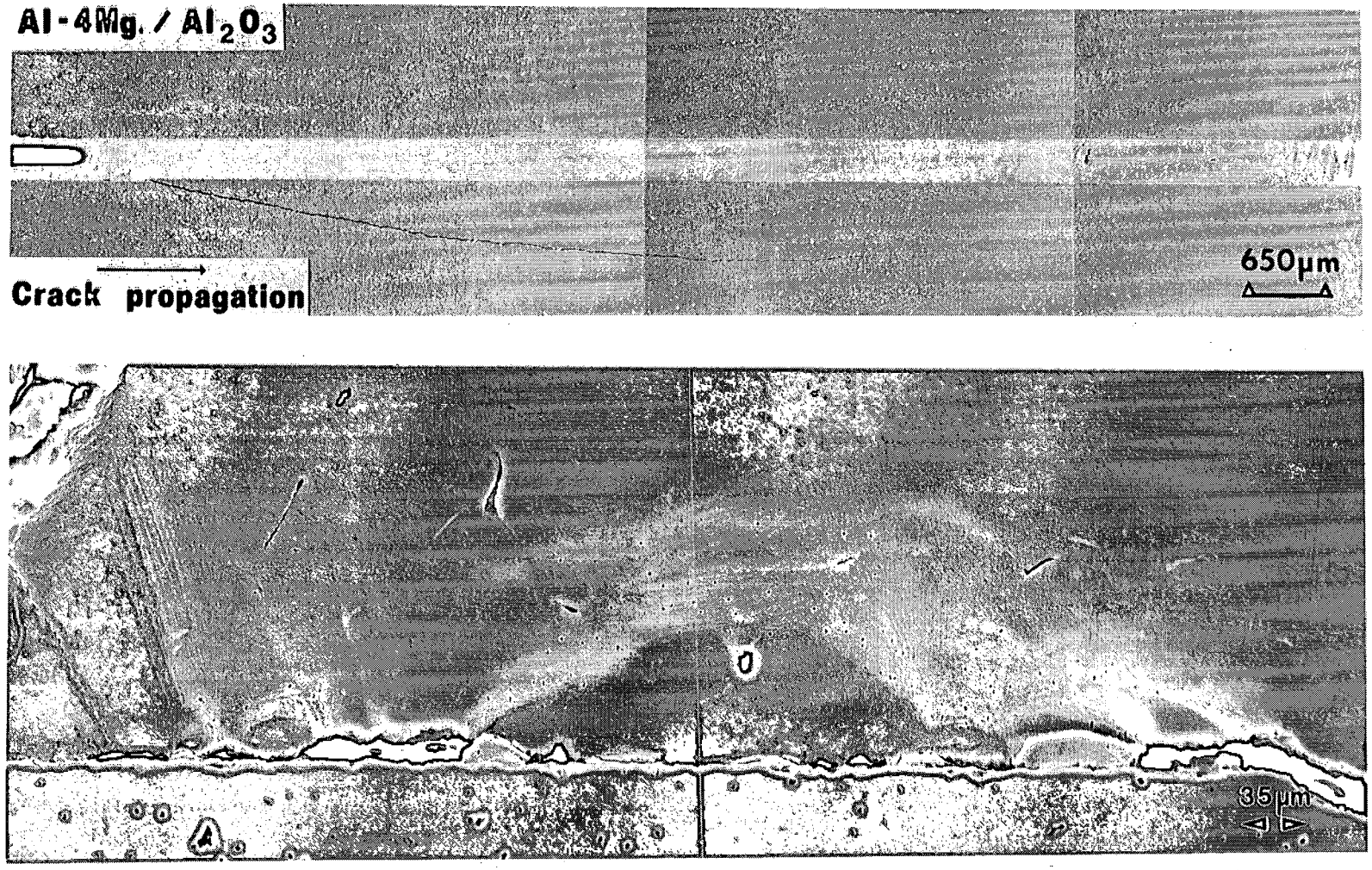

Figure 11: Scanning electron micrographs of the crack-path profiles in Al_2O_3/Al-4Mg C(T) sample ($\beta > 0$), showing a) fatigue-crack initiation at the notch and growth in the metal layer *near* the interface, before final overload failure in the ceramic, and b) higher magnification image of the early fatigue crack growth, showing slip-line activity within the metal layer.

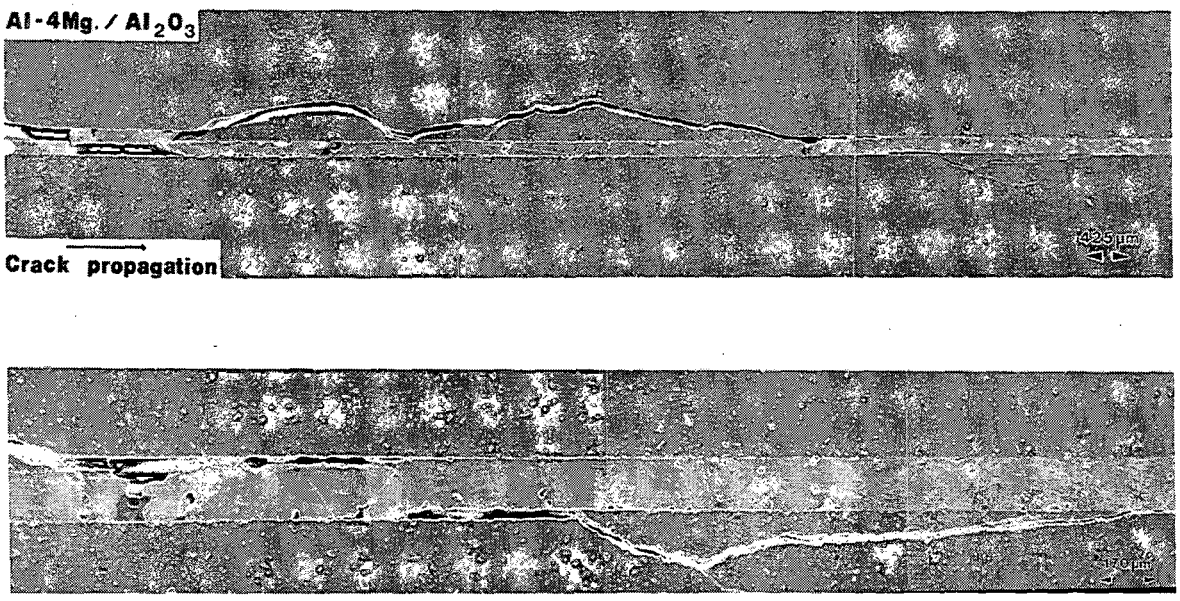

XBB 916-4674

Figure 12: Scanning electron micrographs of the crack-path profile of a fatigue pre-crack and overload failure in Al_2O_3/Al-4Mg C(T) sample ($\beta > 0$), showing examples of crack jumping between interfaces during cyclic crack growth in the metal layer, and overload failure in the ceramic where the crack is continually drawn to the interface.

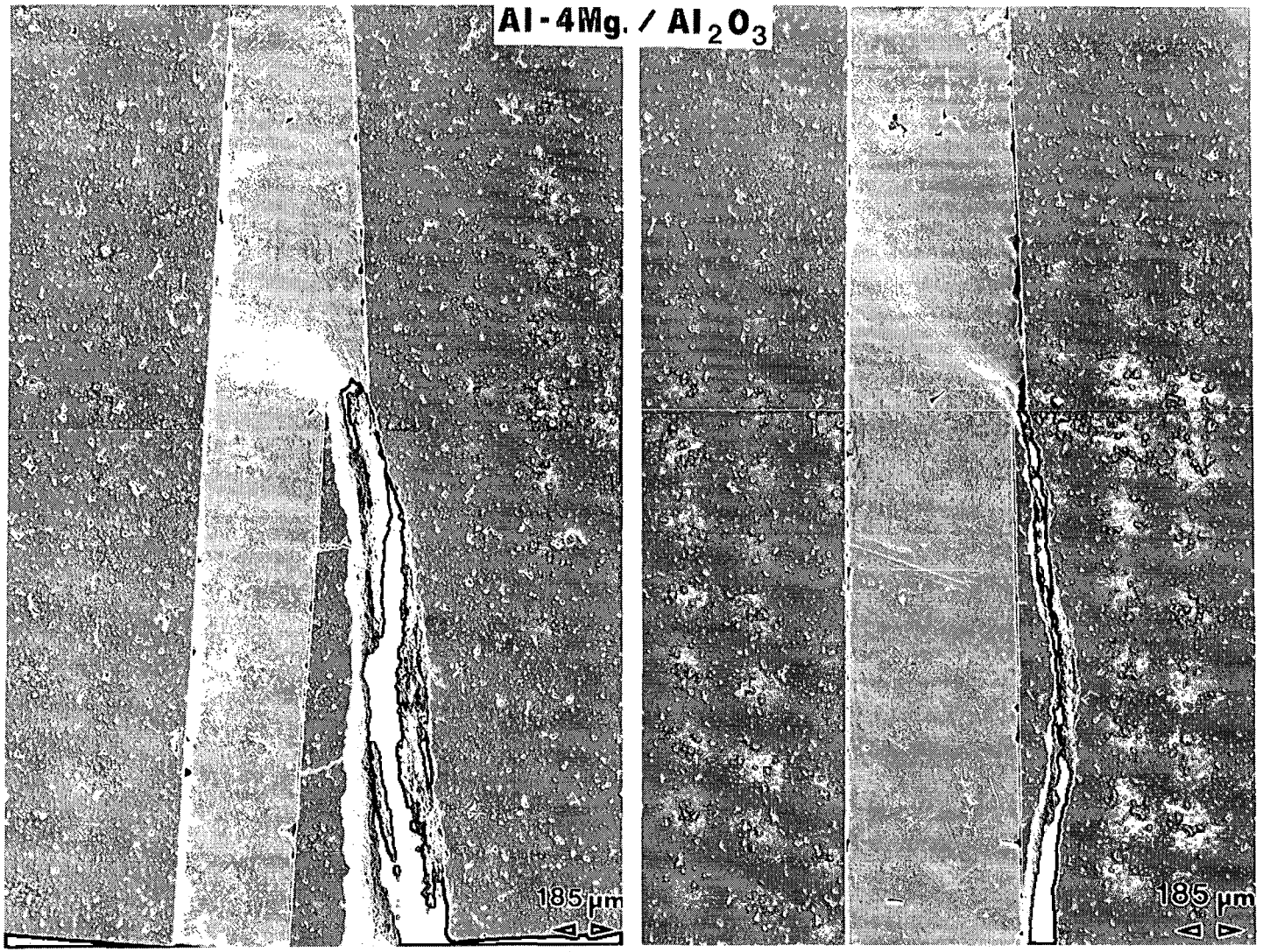

XBB 916-4541

Figure 13: Scanning electron images of sides of Al_2O_3/Al-4Mg/Al_2O_3 ($\beta > 0$) 4-point bend sandwich samples, showing two examples of cracking in the ceramic with cracks being drawn to the layer where they blunt in the metal. Note distinction between these micrographs and those for Al_2O_3/pureAl/Al_2O_3 in Figure 6.

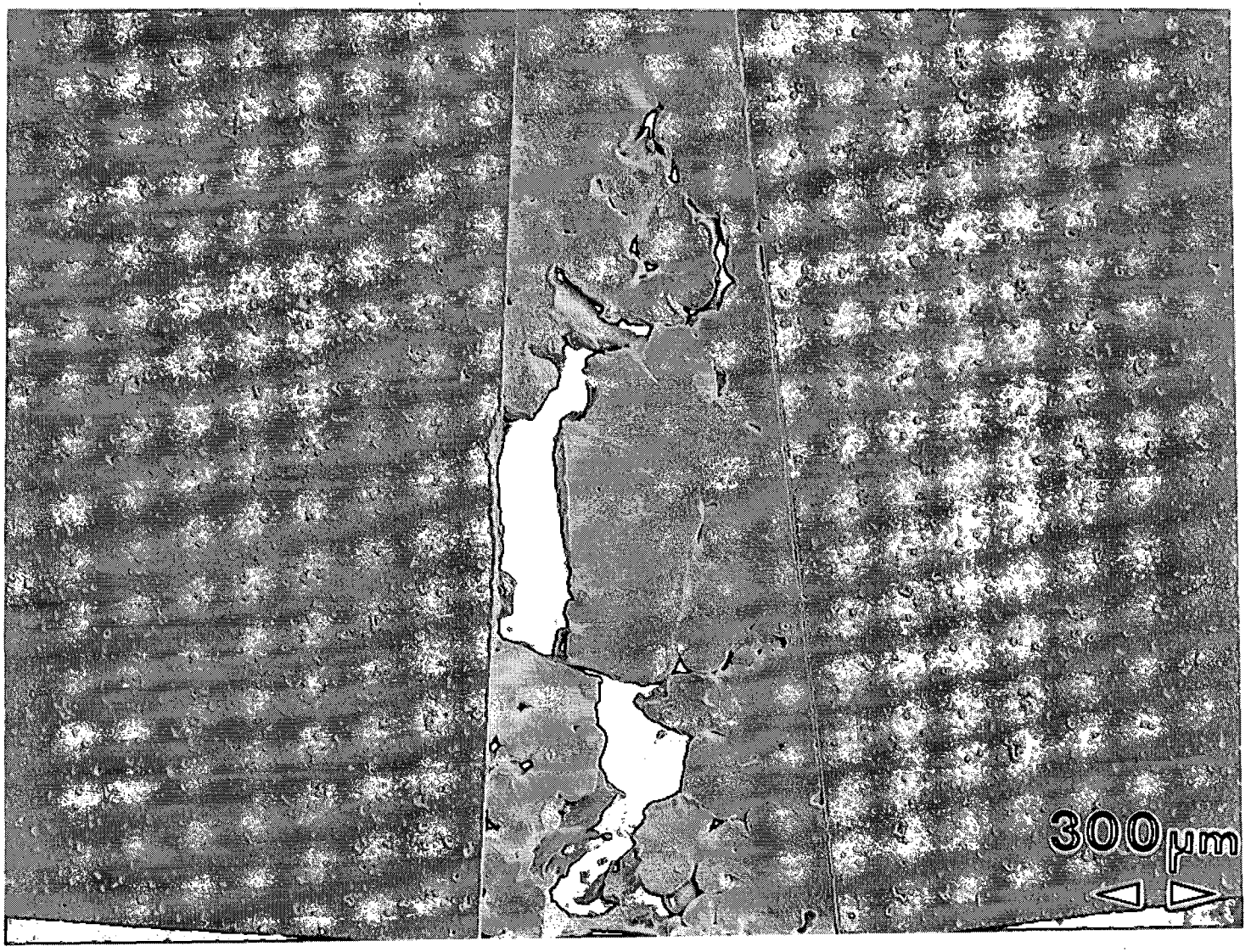

XBB 884-3385

Figure 14: Rare example of crack meandering within the metal layer in Al_2O_3/Cu bend sample.

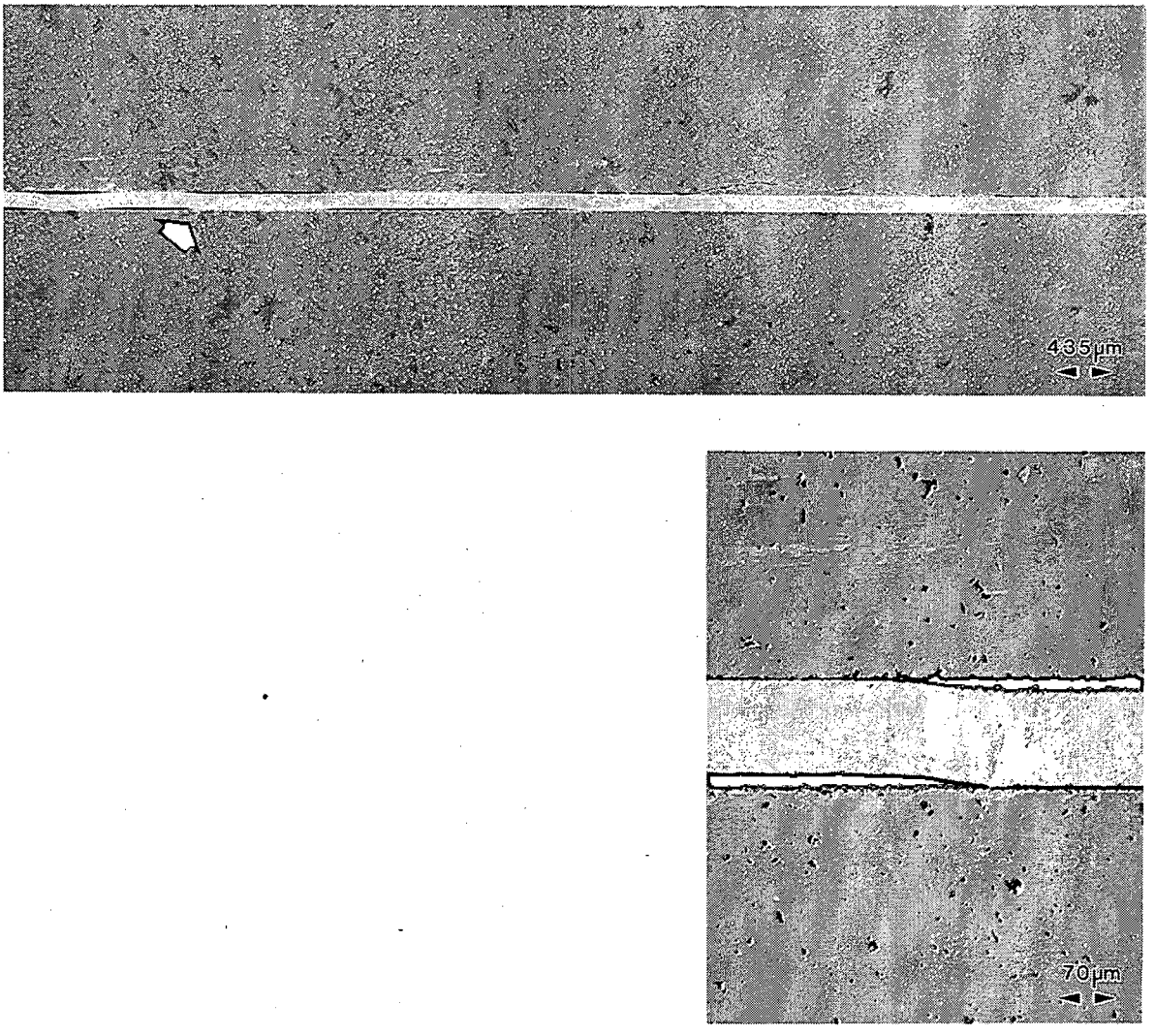

XBB 9110-8436

Figure 15: Low and higher magnification scanning electron images of periodic crack jumping and resulting crack bridging by metal-layer segments during interfacial failure in Al_2O_3/Cu ($\beta > 0$) sandwich specimens.

LAWRENCE BERKELEY LABORATORY
CENTER FOR ADVANCED MATERIALS
1 CYCLOTRON ROAD
BERKELEY, CALIFORNIA 94720